Analytical Study of Transient Coupling between Vessel Motion and Liquid Sloshing in Multiple Tanks

Chongwei Zhang[1]

Abstract: The transient coupling between the vessel motion and liquid sloshing in multiple tanks is investigated. External disturbance factors (e.g., spring constraint or force field) that might affect the oscillation characters of the coupling system are not involved so that the vessel motion is only excited by the liquid sloshing in tanks. The analytical solution for this coupling problem has been derived based on the potential flow theory, which converts the problem to a linear system of ordinary differential equations. The approach to determine natural frequencies of the coupling system is also given. The vessel with one or more rectangular tanks is considered for cases studies. Effects of factors, such as vessel mass, number of tanks, tank configuration and free-surface deformation on the vessel motion, liquid sloshing, and mechanical-energy components of the system are studied systematically. **DOI: 10.1061/(ASCE)EM.1943-7889.0001085.**

Author keywords: Sloshing; Vessel motion; Fluid-structure interaction; Free surface waves; Coupling of sloshing and seakeeping.

Introduction

The liquefied natural gas (LNG) carrier is a vessel designed for transoceanic LNG transportation. After several decades of development, new demands are being raised in the LNG shipping industry. For example, the world's first offshore floating liquefied natural gas (FLNG) facility (i.e., Prelude) is coming soon. During the offloading operation from the FLNG facility to the LNG carrier, the liquid sloshing inside the LNG carrier could have nonneglectable effects on vessel motions (Zhao et al. 2011). Meanwhile, the vessel motions would further excite the liquid sloshing in return. Thus, the interaction between the liquid sloshing and vessel motions forms a coupling problem. What makes the coupling more complicated is that the vessel motion, itself, is also coupled with a complex external environment, such as ocean waves, at the same time. Moreover, each vessel may have multiple liquid tanks so that the liquid motion in each tank could have an interaction with the vessel motion.

At present, simulations on this coupling problem have emerged in the literature, such as in Rognebakke and Faltinsen (2003), Molin et al. (2002), Malenica et al. (2003), Newman (2005), Kim et al. (2007), Mitra et al. (2012) and Zhao et al. (2014). However, because of the complexity of the problem, a systematic understanding of the complete coupling system is still far behind. The complexity is mainly from the inclusion of too many influencing factors (i.e., the external environment, vessel motion, and liquid sloshing in any of the tanks). Thus, to have a deep understanding of this complete problem, it is important to firstly isolate the influencing factors and make clear the coupling mechanism between different pairs of them. The present study would focus on the coupling pair between the liquid sloshing and vessel motions.

[1]Dept. of Mechanical Engineering, Univ. College London, Torrington Place, London WC1E 7JE, U.K. E-mail: chongwei.zhang.11@ucl.ac.uk

Note. This manuscript was submitted on September 17, 2015; approved on January 7, 2016; published online on March 2, 2016. Discussion period open until August 2, 2016; separate discussions must be submitted for individual papers. This paper is part of the ***Journal of Engineering Mechanics***, © ASCE, ISSN 0733-9399.

Studies on the coupling of vessel motion and liquid sloshing in a single tank can be found in some literature. Cooker (1994) has introduced a typical model, which is a single-tank vessel suspended as a bifilar pendulum. Initially, the vessel with still water is dragged away from the equilibrium position before it is released from rest. During the swing motion, the vessel remains horizontal. The swing amplitude, liquid depth, and wave amplitude are all assumed to be small so that the vertical vessel displacement is neglected, and the sloshing could be analyzed using the linear shallow-water theory. It is found that the presence of the sloshing fluid could evidently change the natural oscillation frequency of the suspended system. In recent years, Cooker's model returns to peoples' concern. Alemi Ardakani and Bridges (2010) extended Cooker's theory by including the nonlinear terms in shallow water equations, although the vessel motion is still restricted in a linear sense. They developed a numerical algorithm to solve the coupling problem. Their nonlinear results have shown distinctions from the linear ones in the near resonance situation. Yu (2015) applied the linear finite-depth water theory to Cooker's model. It is found that the shallow-water theory, which assumes the pressure acting on tank walls to be hydrostatic, does not give satisfactory results for cases of shorter suspension length and larger water depth where nonhydrostatic pressure becomes significant. Then, Herczynski and Weidman (2012) performed a related experiment to measure the horizontal oscillation of a vessel solely driven by the liquid sloshing inside. The linear finite-depth solutions are validated by the experiment. Alemi Ardakani et al. (2012) further used a weakly-nonlinear finite-depth water theory for Cooker's model. The resonance, where the natural frequency of the system coincides with one of the fluid modes, was identified. Later, Turner and Bridges (2013) investigated the subtle energy transfer from liquid sloshing to vessel motion through the nonlinearity. Turner et al. (2015) further allowed the pivoting of the vessel with a sloshing tank.

Another model in dealing with the vessel-liquid-coupling problem is the tuned liquid damper (TLD) (a type of liquid tank installed on the top of high buildings to control the wind-induced oscillation). The TLD model is simplified as a liquid vessel constrained by springs and allowed to move freely only in the horizontal direction, which is essentially a mass-spring-damper system. The TLD and Cooker's bifilar pendulum have equivalent governing

equations after linearization but different characteristics in the nonlinear mathematical form. Ikeda and Nakagawa (1997) harmonically excited the TLD model from rest by an electromagnetic exciter. The free surface is weakly-nonlinear. Stability analyses for this nonlinear vibration were performed. Frandsen (2005) studied a similar vibration system. A finite different solver, based on fully-nonlinear potential flow theory, is developed for the flow simulation. The coupling of sloshing and vessel vibration in an external time-varying force field is investigated. Gavrilyuk et al. (2012) derived linear modal equations to study the dynamics of a mechanical system carrying the liquid tank of the tapered conical geometry. Harmonic external forces were also applied.

The previous review suggests that the literature has mainly considered single-tank vessels restrained by suspensions or springs or even placed in time-varying force fields. Studies on the purely free motion of a multiple-tank vessel seem to be rare. Purely, in this case, indicates that external factors (e.g., restoring forces from springs or suspension structures) are not involved. Because either the suspended structure or spring-mass system has an oscillation nature, their existence could totally change oscillation property of a purely coupling system. For example, resonance phenomena may occur if the motion frequency of the vessel with empty tanks coincides with certain natural sloshing frequencies. On the vessel with multiple tanks, two related works are Weidman (2005) and Turner et al. (2013). In their study, the Cooker's experiment with a multi-tank rectangular vessel is examined. Turner et al. (2013) also gave the characteristic equations for the natural frequencies of the coupling problem. However, like most of the aforementioned literature, the problem with the purely free motion is not concerned, neither.

To help fill this gap, the present work would investigate the purely coupling between vessel motions and liquid sloshing in multiple tanks. The vessel is only excited by the liquid sloshing in tanks without external factors that could disturb the oscillation characters of the coupling system. The vessel motion is initially driven by the free-surface deformation in tanks. Based on the potential flow theory, the author would derive the analytical solution of the coupling problem and introduce an approach to determine natural frequencies of the system. Dynamic properties of the coupling system with a single sloshing tank are firstly investigated. Then, multiple sloshing tanks are further involved. The effects of factors, such as vessel mass, number of tanks, and tank configurations, are studied. The present work is a follow-up study of the previous research (e.g., Zhang et al. 2015; Zhang 2015b) on liquid sloshing caused by prescribed excitations.

Problem Descriptions

Consider a vessel with N liquid tanks, as shown in Fig. 1. The tanks are numbered from Tank-1 to Tank-N in sequence. The fluid domain, free surface, and wetted wall in Tank-k ($k = 1$ to N) are denoted by V^k, S_F^k, and S_B^k, respectively. To analyze the liquid sloshing in Tank-k, a tank-fixed coordinate system $O^k - x^k y^k z^k$ is set, with the origin O^k at the center of the mean free surface and $O^k z^k$ axis pointing upward. The earth-fixed coordinate system $O_o - x_o y_o z_o$ is also set, which coincides with the initial position of $O^1 - x^1 y^1 z^1$. The vessel is undergoing a free motion in the $O_o x_o$ direction on the horizontal ground without friction.

The motion of the vessel is determined by the Newton's Second Law

$$m\dot{\mathbf{v}}_c = \sum_{k=1}^{N} \mathbf{F}^k \tag{1}$$

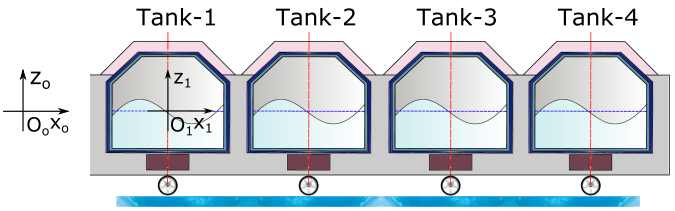

Fig. 1. Sketch of vessel with multiple sloshing tanks

where m = vessel mass without liquid; $\ddot{\mathbf{v}}_c = \{\ddot{v}_1, 0, 0\} = \{\ddot{x}_c, 0, 0\}$ = transversal acceleration of the vessel; and $\mathbf{F}^k = \{F_1^k, 0, 0\}$ = sloshing-induced force from domain V^k. A dot over a variable represents a time derivative. Hereafter, the superscript k indicates that the variable is from the fluid domain in Tank-k. The value of $\mathbf{F}^k$ is from the integration of the pressure over the wetted tank wall S_B^k.

The pressure could be calculated based on the potential flow theory, which assumes the fluid to be inviscid, incompressible, and flow-irrotational. For Tank-k, a scalar velocity potential $\varphi^k(x^k, y^k, z^k, t)$, whose gradient represents the fluid velocity, is introduced. For convenience sake, the superscript k of variables in Tank-k is omitted before calculating hydrodynamic forces. The small-amplitude assumption is further adopted, which requires the amplitude of the liquid and vessel motions to be small relative to the characteristic tank dimension. Then, the velocity potential φ could be determined from the linearized boundary value problem

$$\nabla^2 \varphi = 0, \qquad \text{in } \bar{V} \tag{2}$$

$$\frac{\partial \varphi}{\partial n} = v_1(t) n_1, \qquad \text{on } \bar{S}_B \tag{3}$$

$$\frac{\partial \varphi}{\partial z} = \frac{\partial \eta}{\partial t}, \qquad \text{on } \bar{S}_F \tag{4}$$

$$\eta = -\frac{1}{g}\frac{\partial \varphi}{\partial t}, \qquad \text{on } \bar{S}_F \tag{5}$$

$$\varphi(x, y, z, t) = 0; \qquad \eta(x, y, t) = \bar{\eta}(x, y), \quad \text{for } t \le 0 \tag{6}$$

where $\mathbf{n} = \{n_1, n_2, n_3\}$ = unit normal vector pointing out of the fluid domain; $\eta(x, y, t)$ = free-surface elevation; and g = gravitational acceleration constant. The mean fluid domain, mean wet tank surface, and mean free surface are denoted by $\bar{V}$, $\bar{S}_B$, and $\bar{S}_F$, respectively. The initial conditions in Eq. (6) give the free surface an initial profile. The fluid pressure p is obtained from the linearized Bernoulli's equation

$$p = -\rho \frac{\partial \varphi}{\partial t} - \rho g z + C(t) \tag{7}$$

where ρ = fluid density; and $C(t)$ = spatial-independent function. By redefining φ appropriately, $C(t)$ could be set as zero without affecting the velocity field.

Theoretical Analyses

General Solutions

In this section, the solution of the linearized vessel-liquid-coupling problem is to be derived. The procedure for the liquid sloshing

analysis is similar to that in Zhang (2015a). Firstly, the vessel motion effect is separated from the velocity potential

$$\varphi(x,y,z,t) = v_1(t)x + \phi(x,y,z,t) \tag{8}$$

Substituting Eq. (8) into Eqs. (2)–(5) leads to the boundary value problem of ϕ

$$\nabla^2\phi = 0, \qquad \text{in } \bar{V} \tag{9}$$

$$\frac{\partial\phi}{\partial n} = 0, \qquad \text{on } \bar{S}_B \tag{10}$$

$$\frac{\partial\phi}{\partial z} = \frac{\partial\eta}{\partial t}, \qquad \text{on } \bar{S}_F \tag{11}$$

$$\dot{\phi} + g\eta = -\dot{v}_1 x, \qquad \text{on } \bar{S}_F \tag{12}$$

This is a nonhomogeneous problem whose solution can be written in a summation form

$$\phi(x,y,z,t) = \sum_{i=1}^{\infty} \xi_i(t)\bar{\phi}_i(x,y,z) \tag{13}$$

where $\bar{\phi}_i$ = natural modes of the sloshing liquid; and ξ_i = corresponding time-dependent coefficients. The natural modes $\bar{\phi}_i$ indicate nontrivial solutions of the steady sloshing state. All $\bar{\phi}_i$ form an orthogonal set. Each $\bar{\phi}_i$ corresponds to a natural frequency ω_i, which satisfies the relationship $\partial\bar{\phi}_i/\partial z = (\omega_i^2/g)\bar{\phi}_i$. Because of the conservation of the liquid volume, the following equations are satisfied

$$\int_{\bar{S}_F} \eta dS = 0 \quad \text{or} \quad \int_{\bar{S}_F} \bar{\phi}_i dS = 0 \tag{14}$$

Because Eq. (13) automatically satisfies the Laplace's governing equation and the boundary condition on $\bar{S}_B$, the coefficients ξ_i are only determined by the free-surface conditions on $\bar{S}_F$. Substituting Eq. (13) into Eq. (11) yields

$$\sum_{i=1}^{\infty} \xi_i(t)\frac{\omega_i^2}{g}\bar{\phi}_i = \frac{\partial\eta}{\partial t}, \qquad \text{on } \bar{S}_F \tag{15}$$

So, the following expression can be constructed

$$\eta(x,y,t) = \sum_{i=1}^{\infty} \zeta_i(t)\bar{\phi}_i(x,y,0) \tag{16}$$

Based on the orthogonality of $\bar{\phi}_i$, the following relation is guaranteed

$$\dot{\zeta}_i(t) = \frac{\omega_i^2}{g}\xi_i(t) \tag{17}$$

Further substituting Eqs. (13) and (16) into Eq. (12) leads to

$$\sum_{i=1}^{\infty} [\dot{\xi}_i(t) + g\zeta_i(t)]\bar{\phi}_i = -\dot{v}_1 x, \qquad \text{on } \bar{S}_F \tag{18}$$

or

$$\sum_{i=1}^{\infty} \left[\frac{1}{\omega_i^2}\ddot{\zeta}_i(t) + \zeta_i(t)\right]\bar{\phi}_i = -\frac{1}{g}\dot{v}_1 x, \qquad \text{on } \bar{S}_F \tag{19}$$

Using the orthogonal property, the following linear differential equations could be obtained

$$\frac{1}{\omega_i^2}\ddot{\zeta}_i(t) + \zeta_i(t) = -\frac{\dot{v}_1}{g}\left[\frac{\int_{\bar{S}_F}(x\bar{\phi}_i)dS}{\int_{\bar{S}_F}(\bar{\phi}_i\bar{\phi}_i)dS}\right], \qquad \text{for } i = 1,2,\ldots,\infty \tag{20}$$

Eq. (20) could be rewritten in a neater form

$$\ddot{\zeta}_i(t) + \omega_i^2\zeta_i(t) = -\left(\frac{\omega_i^2}{g}\right)\left(\frac{\lambda_{i1}}{\mu_i}\right)\dot{v}_1, \quad \text{for } i = 1,2,\cdots,\infty \tag{21}$$

with

$$\mu_i = \int_{\bar{S}_F}(\bar{\phi}_i\bar{\phi}_i)dS; \qquad \lambda_{i1} = \int_{\bar{S}_F}(x\bar{\phi}_i)dS \tag{22}$$

Thus, the first relationship between the $\zeta_i(t)$ and $\dot{v}_1$ has been found.

The second relationship exists in the motion equation of the vessel. The hydrodynamic force generated from Tank-k is

$$\begin{aligned} F_1 &= \rho\int_{\bar{S}_B} pn_1 dS = -\rho\int_{\bar{S}_B}\left(\frac{\partial\phi}{\partial t} + gz\right)n_1 dS \\ &= -\rho\int_{\bar{S}_B}\left[\sum_{j=1}^{\infty}\dot{\xi}_j(t)\bar{\phi}_j + \dot{v}_1(t)x + gz\right]n_1 dS \\ &= -\rho\sum_{j=1}^{\infty}\dot{\xi}_j(t)\left(\int_{\bar{S}_B}\bar{\phi}_j n_1 dS\right) - \rho\dot{v}_1(t)\left(\int_{\bar{S}_B} xn_1 dS\right) \\ &\quad - \rho g\left(\int_{\bar{S}_B} zn_1 dS\right) = -\rho g\sum_{j=1}^{\infty}\frac{\ddot{\zeta}_j(t)}{\omega_j^2}\left(\int_{\bar{S}_B}\bar{\phi}_j n_1 dS\right) \\ &\quad - \rho\dot{v}_1(t)\left(\int_{\bar{S}_B} xn_1 dS\right) - \rho g\left(\int_{\bar{S}_B} zn_1 dS\right) \\ &= -\rho g\sum_{j=1}^{\infty}\left(\frac{\gamma_{j1}}{\omega_j^2}\right)\ddot{\zeta}_j(t) - m_l\dot{v}_1(t) - m_z g \end{aligned} \tag{23}$$

with

$$\gamma_{j1} = \int_{\bar{S}_B}\bar{\phi}_j n_1 dS; \qquad m_l = \rho\left(\int_{\bar{S}_B} xn_1 dS\right);$$
$$m_z = \rho\left(\int_{\bar{S}_B} zn_1 dS\right) \tag{24}$$

Substituting F_1^k into Eq. (1) leads to

$$-\rho g\sum_{k=1}^{N}\left\{\sum_{j=1}^{\infty}\left[\frac{\gamma_{j1}^k}{(\omega_j^k)^2}\right]\ddot{\zeta}_j^k(t)\right\} - g\sum_{k=1}^{N} m_z^k = \left(m + \sum_{k=1}^{N} m_l^k\right)\dot{v}_1(t) \tag{25}$$

Note that the superscript k indicating a variable from Tank-k starts to display.

Combine Eqs. (21) and (25) by eliminating the vessel motion $\dot{v}_1$. A series of second-order ordinary differential equations could be obtained

$$\ddot{\zeta}_i^p(t) - \frac{\rho(\omega_i^p)^2}{(m+\sum_{k=1}^N m_l^k)}\left(\frac{\lambda_{i1}^p}{\mu_i^p}\right)\sum_{k=1}^N\left\{\sum_{j=1}^\infty\left[\frac{\gamma_{j1}^k}{(\omega_j^k)^2}\right]\ddot{\zeta}_j^k(t)\right\}$$
$$+(\omega_i^p)^2\zeta_i^p(t) = \frac{(\sum_{k=1}^N m_z^k)}{(m+\sum_{k=1}^N m_l^k)}(\omega_i^p)^2\left(\frac{\lambda_{i1}^p}{\mu_i^p}\right),$$
$$\text{for } i=1,2,\cdots,\infty \quad \text{and} \quad p=1,2,\cdots,N \tag{26}$$

or

$$\ddot{\zeta}_i^p(t) - A_i^p\sum_{k=1}^N\left[\sum_{j=1}^\infty B_j^k\ddot{\zeta}_j^k(t)\right] + C_i^p\zeta_i^p(t) = \left(\sum_{k=1}^N m_z^k\right)A_i^p/\rho;$$
$$m_L = \sum_{k=1}^N m_l^k; \quad A_i^p = \frac{\rho(\omega_i^p)^2}{(m+m_L)}\left(\frac{\lambda_{i1}^p}{\mu_i^p}\right); \quad B_j^k = \left[\frac{\gamma_{j1}^k}{(\omega_j^k)^2}\right];$$
$$C_i^p = (\omega_i^p)^2, \quad \text{for } i=1,2,\cdots,\infty \quad \text{and} \quad p=1,2,\cdots,N \tag{27}$$

The $\zeta_j(t)$ could be solved using typical time stepping methods. Then, the vessel motions could be calculated based on Eq. (25).

Consider the mechanical energy of the oscillation system. The kinetic energy of the vessel is defined as

$$E_K^0(t) = \frac{1}{2}mv_1^2 \tag{28}$$

The potential energy E_P^k and kinetic energy E_K^k of the liquid in Tank-k have the expression

$$E_K^k(t) = \frac{\rho}{2}\int\int\int_{\overline{V}^k}(\nabla\varphi^k\cdot\nabla\varphi^k)dV = \frac{\rho}{2}\int\int_{\overline{S}_F^k+\overline{S}_B^k}\varphi^k\nabla\varphi^k\cdot\mathbf{n}dS$$
$$= \frac{\rho}{2}\int\int_{\overline{S}_F^k+\overline{S}_B^k}\varphi^k\varphi_n^k dS \tag{29}$$

$$E_P^k(t) = \frac{\rho g}{2}\int\int_{\overline{S}_F^k}(\eta^k)^2 dS \tag{30}$$

Case of Rectangular Tanks

In the previous derivations, the tank geometry is not restricted. To solve Eq. (27), natural sloshing frequencies/modes for each tank must be known. One may refer to Zhang (2015a) for the calculation of natural frequencies/modes for a liquid tank of general geometry. In the present study, the author would focus on the vessel with rectangular tanks. Possible natural frequencies and corresponding modes for the sloshing in Tank-k could be found analytically

$$\omega_j^k = \sqrt{gk_j^k\tanh[k_j^kH^k]}, \quad \text{with } k_j^k = j\pi/L^k \tag{31}$$

$$\bar{\phi}_j^k(x^k,y^k,z^k) = \frac{\cosh[k_j^k(z^k+H^k)]}{\cosh(k_j^kH^k)}\cos[k_j^k(x^k+L^k/2)];$$
$$\bar{\phi}_j^k(x^k,y^k,0) = \cos[k_j^k(x^k+L^k/2)] \tag{32}$$

where L^k and H^k = length and averaged liquid depth of Tank-k. The integrations in Eq. (27) can be calculated analytically

$$\mu_i^k = L^k/2; \qquad \lambda_{i1}^k = [\cos(i\pi)-1]/(k_i^k)^2 = [(-1)^i-1]/(k_i^k)^2;$$
$$m_l^k = \rho L^kH^k; \qquad m_z^k = 0;$$
$$\gamma_{j1}^k = \frac{\cos(j\pi)-1}{k_j^k}\tanh(k_j^kH^k) = \frac{(-1)^j-1}{k_j^k}\tanh(k_j^kH^k) \tag{33}$$

So, Eq. (27) could be written as

$$\ddot{\zeta}_i^p(t) - A_i^p\sum_{k=1}^N\left[\sum_{j=1}^\infty B_j^k\ddot{\zeta}_j^k(t)\right] + C_i^p\zeta_i^p(t) = 0;$$
$$A_i^p = \frac{2\rho[(-1)^i-1]}{L^p(m+m_L)}\left(\frac{\omega_i^p}{k_i^p}\right)^2; \qquad B_j^k = \left(\frac{1}{k_j^k}\right)^2\left[\frac{(-1)^j-1}{g}\right];$$
$$C_i^p = (\omega_i^p)^2, \quad \text{for } i=1,2,\cdots,\infty \quad \text{and} \quad p=1,2,\cdots,N \tag{34}$$

Because $\zeta_i^k(t)\equiv 0$ for $i=2,4,6,\cdots$, Eq. (34) could be further simplified as

$$A_i^p\sum_{k=1}^N\left[\sum_{j=1}^\infty B_j^k\ddot{\zeta}_j^k(t)\right] - \ddot{\zeta}_i^p(t) = C_i^p\zeta_i^p(t),$$
$$\text{for } i=1,3,5,7,\cdots,\infty, \qquad j=1,3,5,7,\cdots,\infty$$
$$\text{and} \quad p=1,2,\cdots,N \tag{35}$$

with

$$A_i^p = -\left(\frac{4\rho}{L^p}\right)\frac{1}{(m+m_L)}\left(\frac{\omega_i^p}{k_i^p}\right)^2;$$
$$B_j^k = -\left(\frac{2}{g}\right)\left(\frac{1}{k_j^k}\right)^2; \qquad C_i^p = (\omega_i^p)^2 \tag{36}$$

For the solvability, finite terms in Eq. (35) should be chosen. Here is an example. If the first two active modes in three tanks are taken by letting $i=1,3$, $j=1,3$, and $N=3$, the second-order ordinary differential equation could be expressed in the following matrix form

$$\begin{bmatrix} A_1^1B_1^1-1 & A_1^1B_1^2 & A_1^1B_1^2 & A_1^1B_2^2 & A_1^1B_1^3 & A_1^1B_2^3 \\ A_2^1B_1^1 & A_2^1B_2^1-1 & A_2^1B_1^2 & A_2^1B_2^2 & A_2^1B_1^3 & A_2^1B_2^3 \\ A_1^2B_1^1 & A_1^2B_2^1 & A_1^2B_1^2-1 & A_1^2B_2^2 & A_1^2B_1^3 & A_1^2B_2^3 \\ A_2^2B_1^1 & A_2^2B_2^1 & A_2^2B_1^2 & A_2^2B_2^2-1 & A_2^2B_1^3 & A_2^2B_2^3 \\ A_1^3B_1^1 & A_1^3B_2^1 & A_1^3B_1^2 & A_1^3B_2^2 & A_1^3B_1^3-1 & A_1^3B_2^3 \\ A_2^3B_1^1 & A_2^3B_2^1 & A_2^3B_1^2 & A_2^3B_2^2 & A_2^3B_1^3 & A_2^3B_2^3-1 \end{bmatrix}\begin{Bmatrix} \ddot{\zeta}_1^1 \\ \ddot{\zeta}_3^1 \\ \ddot{\zeta}_1^2 \\ \ddot{\zeta}_3^2 \\ \ddot{\zeta}_1^3 \\ \ddot{\zeta}_3^3 \end{Bmatrix} = \begin{Bmatrix} C_1^1\zeta_1^1 \\ C_3^1\zeta_3^1 \\ C_1^2\zeta_1^2 \\ C_3^2\zeta_3^2 \\ C_1^3\zeta_1^3 \\ C_3^3\zeta_3^3 \end{Bmatrix} \tag{37}$$

Known $\ddot{\zeta}_j^k$, the acceleration of the vessel could be calculated by

$$\dot{v}_1(t) = -\frac{\rho g}{(m+m_L)}\sum_{k=1}^N\left[\sum_{j=1}^\infty B_j^k\ddot{\zeta}_j^k(t)\right], \quad \text{for } j=1,3,5,7,\cdots,\infty \tag{38}$$

J. Eng. Mech., 2016, 142(7): -1--1

where m = vessel mass without liquid; and m_L = total mass of the liquid in all tanks. The velocity and displacement of the vessel could be further calculated based on time integration methods.

Natural Frequencies of Coupling System

For the concerned coupling system, there might be a situation in which the vessel and liquid in all tanks oscillate with the same frequency ω. Then, the ω is the natural frequency of the coupling system. It is noted that Turner et al. (2013) investigated the Cooker's experiment with a multicompartment vessel and gave the characteristic equation with respect to the vessel motion frequencies. In a limit case when the suspended string length is infinite, their solution could be applied to the present problem. This subsection would provide an alternative derivation for the natural frequencies, based on the cosine-type expansions as in Eq. (32).

For the periodic oscillations with frequency ω, the expression $\zeta_i^k(t) = \overline{\zeta}_i^k \sin(\omega t)$ may be set. Thus, Eq. (35) could be reformed as

$$-\omega^2 \sin(\omega t) A_i^p \sum_{k=1}^{N}\left(\sum_{j=1}^{\infty} B_j^k \overline{\zeta}_j^k\right) + \overline{\zeta}_i^p \omega^2 \sin(\omega t) = C_i^p \overline{\zeta}_i^p \sin(\omega t),$$
$$\text{for } i = 1,3,5,7,\cdots,\infty, \qquad j = 1,3,5,7,\cdots,\infty \quad \text{and}$$
$$p = 1,2,\cdots,N \tag{39}$$

i.e.

$$-\omega^2 A_i^p \sum_{k=1}^{N}\left(\sum_{j=1}^{\infty} B_j^k \overline{\zeta}_j^k\right) + (\omega^2 - C_i^p)\overline{\zeta}_i^p = 0,$$
$$\text{for } i = 1,3,5,7,\cdots,\infty, \qquad j = 1,3,5,7,\cdots,\infty \quad \text{and}$$
$$p = 1,2,\cdots,N \tag{40}$$

Accordingly, the matrix form in Eq. (37) could be expressed as

$$[M(\omega)]\{\overline{\zeta}_1^1, \overline{\zeta}_3^1, \overline{\zeta}_1^2, \overline{\zeta}_3^2, \overline{\zeta}_1^3, \overline{\zeta}_3^3\}^T = 0 \tag{41}$$

$$[M(\omega)] = \omega^2 \begin{bmatrix} A_1^1B_1^1 - 1 & A_1^1B_2^1 & A_1^1B_1^2 & A_1^1B_2^2 & A_1^1B_1^3 & A_1^1B_2^3 \\ A_2^1B_1^1 & A_2^1B_2^1 - 1 & A_2^1B_1^2 & A_2^1B_2^2 & A_2^1B_1^3 & A_2^1B_2^3 \\ A_1^2B_1^1 & A_1^2B_2^1 & A_1^2B_1^2 - 1 & A_1^2B_2^2 & A_1^2B_1^3 & A_1^2B_2^3 \\ A_2^2B_1^1 & A_2^2B_2^1 & A_2^2B_1^2 & A_2^2B_2^2 - 1 & A_2^2B_1^3 & A_2^2B_2^3 \\ A_1^3B_1^1 & A_1^3B_2^1 & A_1^3B_1^2 & A_1^3B_2^2 & A_1^3B_1^3 - 1 & A_1^3B_2^3 \\ A_2^3B_1^1 & A_2^3B_2^1 & A_2^3B_1^2 & A_2^3B_2^2 & A_2^3B_1^3 & A_2^3B_2^3 - 1 \end{bmatrix} + \begin{bmatrix} C_1^1 & & & & & 0 \\ & C_3^1 & & & & \\ & & C_1^2 & & & \\ & & & C_3^2 & & \\ & & & & C_1^3 & \\ 0 & & & & & C_3^3 \end{bmatrix} \tag{42}$$

For the homogeneous system in Eq. (41), it is known that nonzero solutions exist only if the determinant of the matrix $[M(\omega)]$ is zero, i.e.,

$$\det[M(\omega)] = 0 \tag{43}$$

All values of ω that could guarantee Eq. (43) are natural frequencies of the coupling system. The root of Eq. (43) could be determined from the diagram of the determinant of $[M(\omega)]$ with respective to ω.

The acceleration of the vessel has the form

$$\dot{v}_1(t) = \frac{\rho g \omega^2}{(m + m_L)} \sum_{k=1}^{N}\left(\sum_{j=1}^{\infty} B_j^k \overline{\zeta}_i^k\right) \sin(\omega t),$$
$$\text{for } j = 1,3,5,7,\cdots,\infty \tag{44}$$

from which the amplitude of the motion could be known.

Accuracy Comparison

To verify the accuracy of present derivations, the experimental case in Herczynski and Weidman (2012) is adopted for comparison. The model is a vessel with a rectangular liquid tank on a horizontal frictionless ground. The tank has length $L = 0.2474$ m and width $B = 0.08255$ m, and the vessel with an empty tank has weight $m = 0.8865$ kg. In order to achieve the low-friction situation in the experiment, the vessel is outfitted with four knife-edge wheels that would rotate freely on high-quality ball bearings. Firstly, the vessel is manually oscillated in the length direction so that the free-surface profile of the first or second antisymmetric mode [i.e., $j = 1$ or $j = 3$ in Eq. (32)] could turn up. Then, set the vessel free.

The analytical solution of this problem could be obtained by setting the initial conditions as

$$\zeta_j(0) = A; \quad \dot{\zeta}_j(0) = 0; \quad x_c(0) = 0; \quad \dot{x}_c(0) = 0 \tag{45}$$

which means that the vessel is initially stationary, and the free surface has a cosine-type initial profile

$$\eta(x, y, 0) = A\cos[k_j(x + L/2)] \tag{46}$$

The first and second antisymmetric mode of the free-surface profile are achieved by employing $j = 1$ and $j = 3$, respectively. In this calculation, truncating 20 terms in the expansion of Eq. (16) could provide a sufficient convergence of the result, which is seen in Fig. 5. When set free, the vessel would undergo an oscillation solely excited by sloshing pressure forces inside the tank. Time histories of the wave elevation and vessel displacement could be obtained. Dominant oscillation frequencies of the fluid and vessel are evaluated by the fast Fourier transform (FFT).

Present analytical results are compared with theoretical solutions and experimental data from Herczynski and Weidman

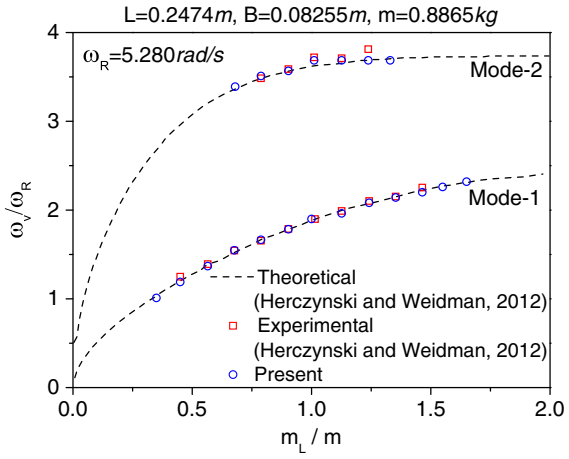

Fig. 2. Oscillation frequency of single-tank vessel, with initial free-surface deformation of Mode-1 and Mode-2, for $L = 0.2474$ m, $B = 0.08255$ m, $m = 0.8865$ kg, and $\omega_R = 5.280$ rad/s

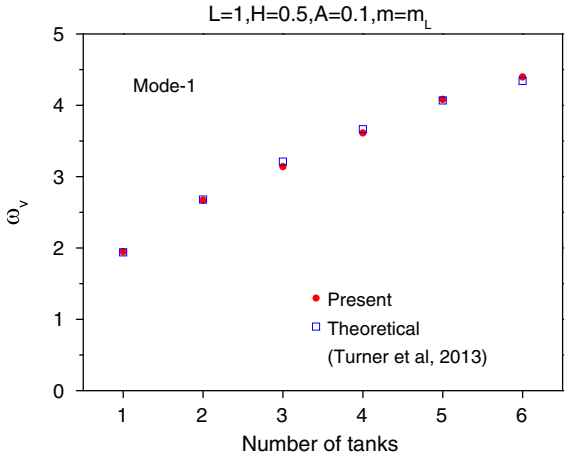

Fig. 3. Oscillation frequency of multiple-tank vessel, with initial free-surface deformation of Mode-1 in Tank-1, for $L = 1$, $H = 0.5$, $m = m_L$, and $A = 0.1$

(2012), which are shown in Fig. 2. This figure shows oscillation frequencies of the vessel with different liquid-filling depths. Mode-1 and Mode-2 indicate that the initial free surface has the deformation of the first and second antisymmetric mode, respectively. The ω_v denotes the dominant oscillation frequency of the vessel, and ω_R is a reference frequency computed in the literature for normalization. The liquid mass m_L varies by adjusting the liquid depth H. It is observed that the present results have a good agreement with the theoretical and experimental results from the literature, which has indicated the accuracy of the present derivation. Additionally, it is found that the frequency of the vessel motion increases with the liquid depth. As the liquid becomes deeper, the variation of the oscillation frequency slows down, which is more evident for the case of Mode-2. More systematic analysis on the free motion of a single-tank vessel is given in the next section.

Hereafter, all results are nondimensionalized. Assume that all tanks on the vessel have the same height H_t and width B. Meanwhile, $B = H_t$. The tank height H_t as well as the gravity acceleration g and liquid density ρ are used as bases of the nondimensionalization. To be specific, variables are nondimensionalized as $(x, y, z, L, B, H, A, \eta) \to (x, y, z, L, B, H, A, \eta)H_t$, $t \to \tau\sqrt{H_t/g}$, and $\omega \to \omega\sqrt{g/H_t}$.

The vessel with multiple tanks is also considered. Firstly, a single-tank vessel is settled. The tank has length $L = 1$ and mean liquid depth $H = 0.5$. The vessel mass equals the liquid mass. Then, nonporous baffles are inserted into the tank, leading to multiple uniform subtanks. Here, the vessel with 6 subtanks in maximum is considered. The vessel motion is initially excited by the free-surface deformation of Mode-1 in a subtank. The theoretical solution derived by Turner et al. (2013) could be applied to verify present results. In Fig. 3, the vessel motion frequencies obtained from the FFT method and the theoretical solution are compared. Corresponding results have shown fairly good agreements. Thus, the accuracy of the present derivation is verified.

The following sections focus on the coupling between the vessel motion and liquid sloshing in either single or multiple tanks. Any external factor that might disturb the oscillation characters of the coupling system is not included from beginning to end. Thus, the free surface is still given an initial deformation as Eq. (46) to drive the vessel motion, instead of artificially oscillating the vessel for an amount of time.

It is known that, for a stationary tank, giving the free surface an initial deformation as Eq. (46) would lead to a steady free-surface oscillation, which means that the free surface would oscillate periodically with invariable amplitude at a unique frequency. This is caused by the fact that Eq. (46) has the exact form of a sloshing mode for the stationary tank. However, when the tank is not fixed and allowed to move freely, the steady state may not occur. Because the sloshing mode in a freely moving vessel is expected to be different from that in the stationary tank. As a result, more than one frequency component might be observed in the results.

Free Motion of Vessel with a Single Liquid Tank

Example Description

In this section, the free motion of a single-tank vessel is considered. The first case aims to give an intuitive description of the vessel-fluid coupling procedure before systematic analysis. The vessel holds a tank of dimensions $L = B = 1$ and liquid depth $H = 0.5$. The free surface has an initial profile of the fundamental mode with amplitude $A = 0.1$. Note that, for the linear problem, the amplitude A could not affect the oscillation frequencies of the solution. Let $m = m_L$. The vessel positions and free-surface profiles in the tank within the first period are shown in Fig. 4. The initial tank motion is motivated by the asymmetric distribution of the static pressure on side walls. As the tank moves toward the left, the waterline along the right tank wall rises. The time of this maximum runup coincides with that of the extreme displacement of the tank. Thus, the vessel motion and wave sloshing in the situation are in an antiphase status, according to Cooker (1994). This antiphase character is different from that of Cooker's (1994) suspended system. For the suspended system, the gravity provides the restoring force directly in concert with or in opposition to the hydrodynamic force so that both in-phase and antiphase oscillations can occur. When the suspension length tends to infinity, only the antiphase mode becomes dominant.

Fig. 5 gives the time history of the vessel displacement and the wave elevation along the right tank wall. The first 20 and 40 terms in the expansion of Eq. (16) are adopted, respectively. For either the vessel displacement or the wave elevation, results from two truncation options coincide graphically. Thus, the 20-term truncation could provide a sufficient convergence of the result. From Fig. 5,

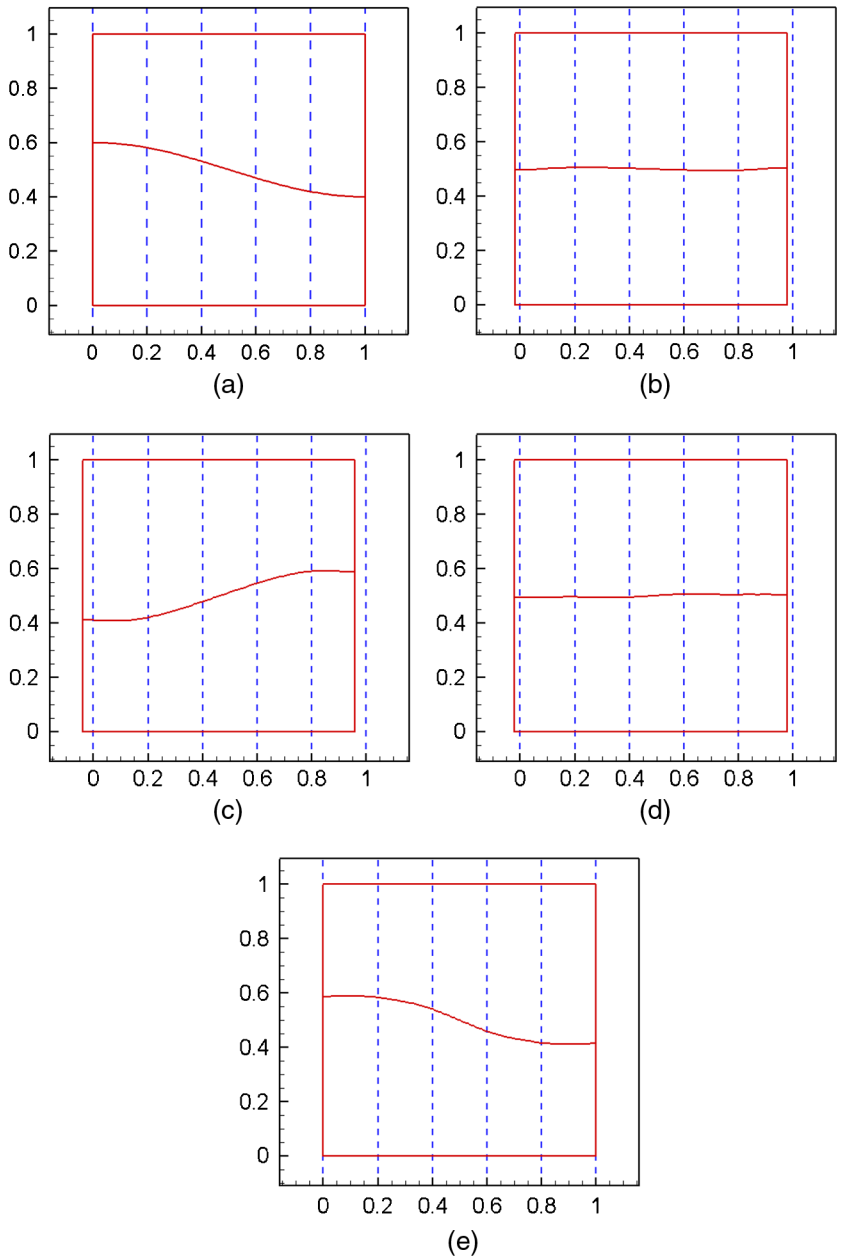

Fig. 4. Position and free-surface profiles for single-tank vessel, with initial free-surface deformation of Mode-1, for $L = 1$, $H = 0.5$, $m = m_L$, and $A = 0.1$, at: (a) $\tau = 0$; (b) $\tau = 0.8$; (c) $\tau = 1.6$; (d) $\tau = 2.4$; (e) $\tau = 3.2$

it is observed that the vessel is undergoing a nearly harmonic oscillation. However, the oscillation of waves is not strictly harmonic. Fig. 6(a) shows the corresponding spectra of both time histories. It is clear that the frequency dominating the wave and vessel motions is ω_{v1}. However, in the spectrum of the wave elevation history, higher frequencies ω_{v2}, ω_{v3}, and ω_{v4} could also be observed. Fig. 6(b) is the diagram of $\det[M(\omega)]$ for this system, from which it can be found that ω_{v1} to ω_{v4} are all natural frequencies of the coupling system. The occurrence of these higher-order frequencies in this linear system is caused by the initial conditions. As mentioned previously, this initial free-surface deformation is not the 'true' free-surface mode of this coupling system. The adopted initial free-surface deformation could be represented by a summation of true free-surface modes corresponding to each ω_v. According to the superposition principle, more than one natural frequency could be observed in the spectrum of the time history.

Fig. 7 shows the mechanical-energy components of the system. The proportion changing of the vessel's kinetic energy E_K^0, fluid's kinetic energy E_K, and fluid's potential energy E_P during the vessel vibration varies with time. Because this is an isolated system, which is only subject to conservative forces, the principle of conservation of mechanical energy is guaranteed. From Fig. 7, it is observed that the summation of E_K^0, E_K, and E_P is not exactly constant but shaking slightly as time going on. This is because the integration in Eq. (29) for the calculation of E_K is performed on the mean fluid boundary instead of the exact one, based on the linear approximation. The kinetic and potential energy are always antiphase, as expected. Also, the oscillation frequency of the kinetic/potential energy is two times that of the vessel motion. This could be understood easily. For example, the potential energy could reach a maximum value at the left and right extreme of the vessel position. It is interesting to find that the kinetic energy of the vessel and fluid are

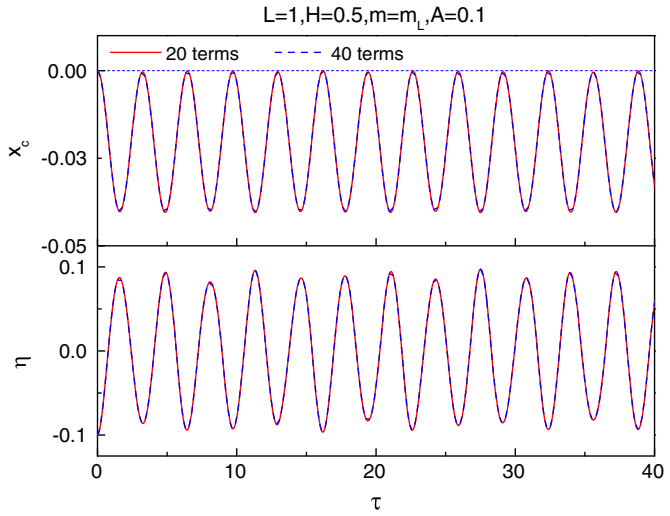

Fig. 5. Displacement of single-tank vessel and wave elevation along the right tank wall, with initial free-surface deformation of Mode-1, for $L = 1$, $H = 0.5$, $m = m_L$, and $A = 0.1$

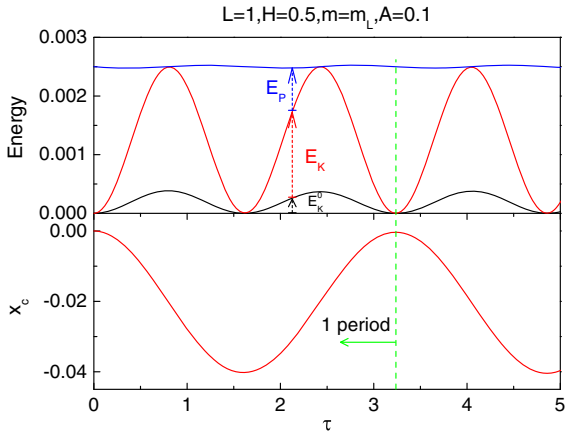

Fig. 7. Energy analysis for single-tank vessel, with initial free-surface deformation of Mode-1, for $L = 1$, $H = 0.5$, $m = m_L$, and $A = 0.1$

in phase. This suggests that as the potential energy reaches maximum, both the vessel and fluid are still at the same time. Also, when the free surface becomes flat, the potential energy is totally transformed into the kinetic energy of the vessel and fluid.

Effects of Vessel Mass

In the second case, effects of the vessel mass are considered. The free surface in the tank also has an initial deformation of Mode-1, with $A = 0.1$. As noticed in Fig. 5, the vessel oscillates in a nearly harmonic way. Then, the dominant frequency ω and averaged amplitude A_c of the vessel oscillation could be obtained through FFT. Fig. 8 shows the obtained ω and A_c when the vessel mass varies from $m = 0.01m_l$ to $m = 20m_l$. As the vessel mass increases, it is found that (1) the vessel motion amplitude decreases and gradually approaches zero; and (2) the rate of this amplitude decrease slows down evidently. This could be explained from Eq. (44). Once the liquid domain and initial conditions are known, values of the liquid mass and other parameters in Eq. (44) are fixed. Thus, the motion amplitude and vessel mass has a near reciprocal relationship. For the oscillation frequency of the vessel motion, it is observed that the oscillation frequency of the freely moving vessel is always higher than the fundamental natural sloshing frequency ω_1 in the fixed tank. As the mass ratio grows, the motion frequency has a decreasing trend similar to that of the motion amplitude. At $m = 20m_l$, the ω has become very close to ω_1. On this point, the vessel-liquid system has the similarity with the mass-spring system whose natural oscillation frequency decreases with the mass.

Effects of Tank Configuration

In Figs. 2 and 8, the mass ratio of the liquid and vessel has been taken as the variable. However, even for a constant mass ratio, the tank configuration (i.e., tank length L and liquid depth H) could affect the oscillation properties. Thus, the third case would investigate the effects of tank configurations on vessel motions. The author would fix the mass of the vessel and the liquid and increase the tank length L from 0.25 to 3.5. Correspondingly, the liquid depth H decreases from 2.0 to 0.14. Assume that the liquid could never spill out or impact the tank roof. The initial free-surface deformation is as Mode-1 with $A = 0.1$. Fig. 9 gives the free-surface elevation histories along the right tank wall of different tanks. It shows that sloshing waves in different tanks generally have similar amplitudes, especially for tanks with deep liquid ($H > 0.5$). However, waves in these tanks have apparently different oscillation frequencies. The

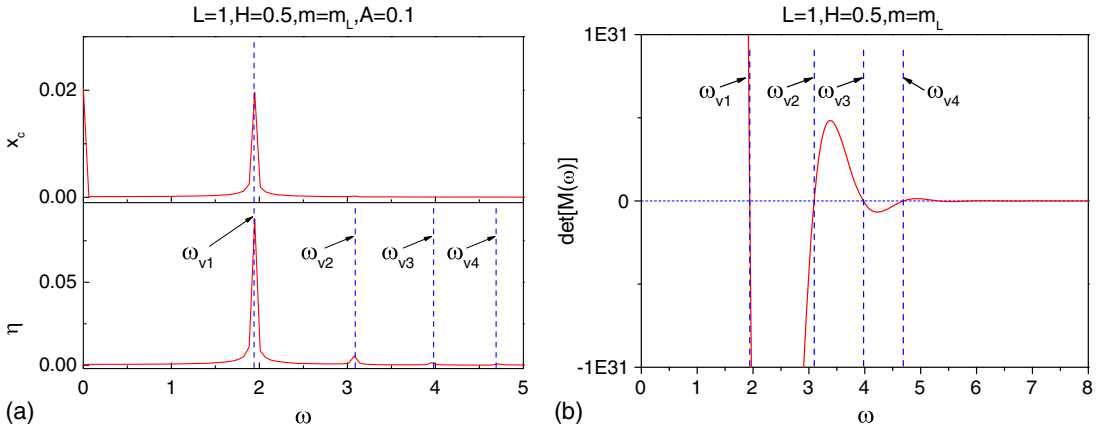

Fig. 6. Frequency analysis for single-tank vessel, with initial free-surface deformation of Mode-1, for $L = 1$, $H = 0.5$, and $m = m_L$: (a) spectrum of vessel displacement and wave elevation along the right tank wall, with $A = 0.1$; (b) diagram of $\det[M(\omega)]$

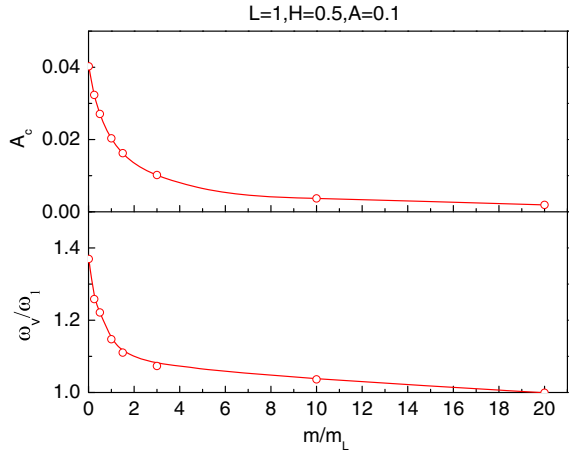

Fig. 8. Effect of vessel mass on oscillation amplitude and frequency of single-tank vessel, with initial free-surface deformation of Mode-1, for $L = 1$, $H = 0.5$, and $A = 0.1$

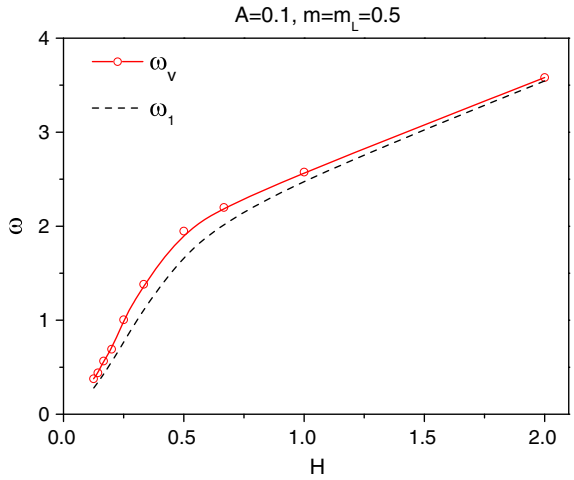

Fig. 10. Effect of tank configuration on oscillation frequency of single-tank vessel, with initial free-surface deformation of Mode-1, for $m = m_L = 0.5$ and $A = 0.1$

dominant oscillation frequencies of the free surface elevation in an either freely moving or fixed vessel are compared in Fig. 10. The sloshing frequency in the freely moving vessel is always higher than that in a fixed vessel, which is expected from the observation in Fig. 8.

Histories of the vessel motion are shown in Fig. 11. It is clear that the motion amplitude increases greatly as the liquid gets shallower. Eq. (44) could be used to explain this. The analytical expression of the vessel displacement amplitude for this case could be approximated as

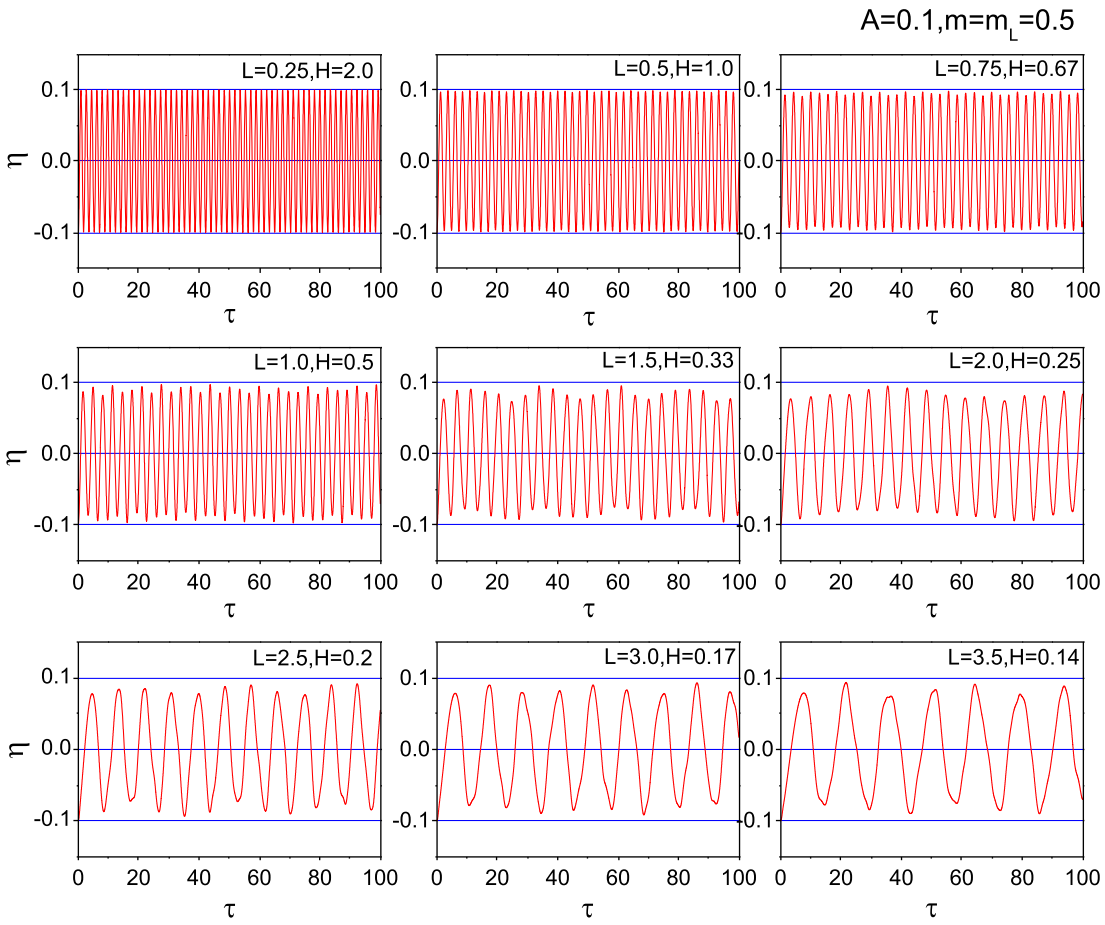

Fig. 9. Effect of tank configuration on wave elevation history in single-tank vessel, with initial free-surface deformation of Mode-1, for $m = m_L = 0.5$ and $A = 0.1$

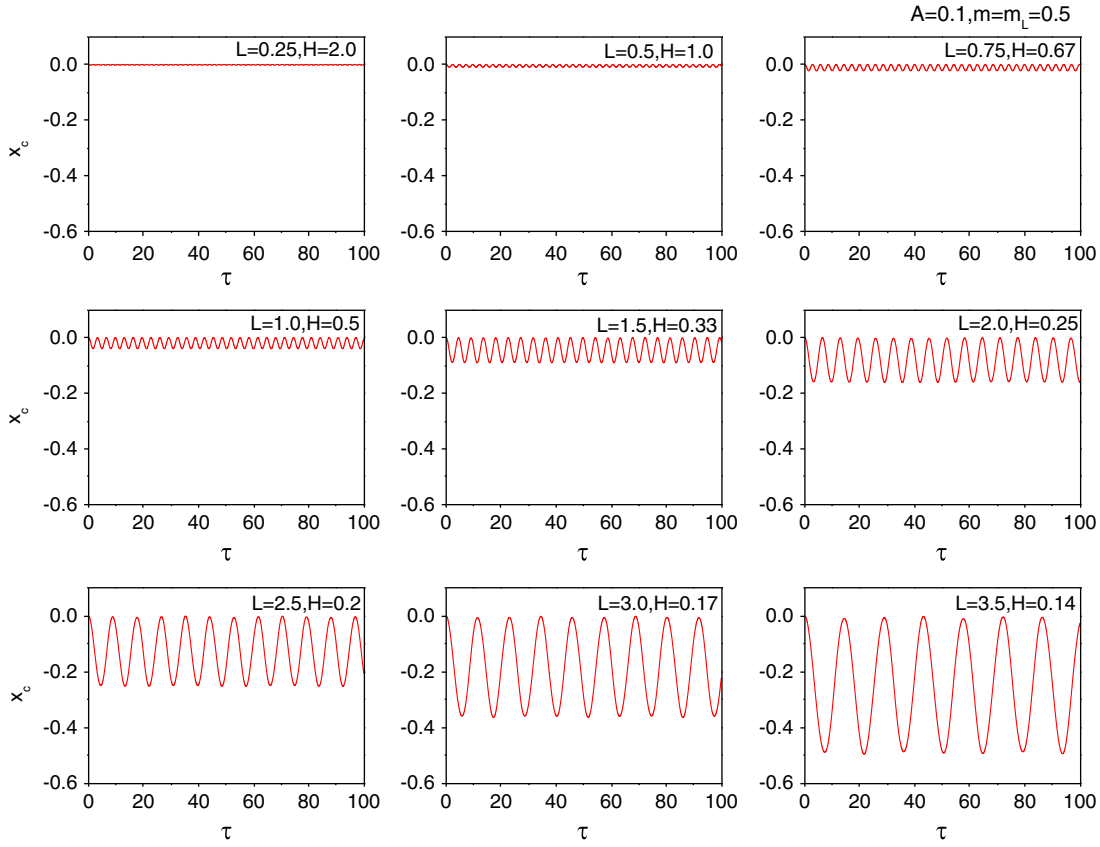

Fig. 11. Effect of tank configuration on displacement of single-tank vessel, with initial free-surface deformation of Mode-1, for $m = m_L = 0.5$ and $A = 0.1$

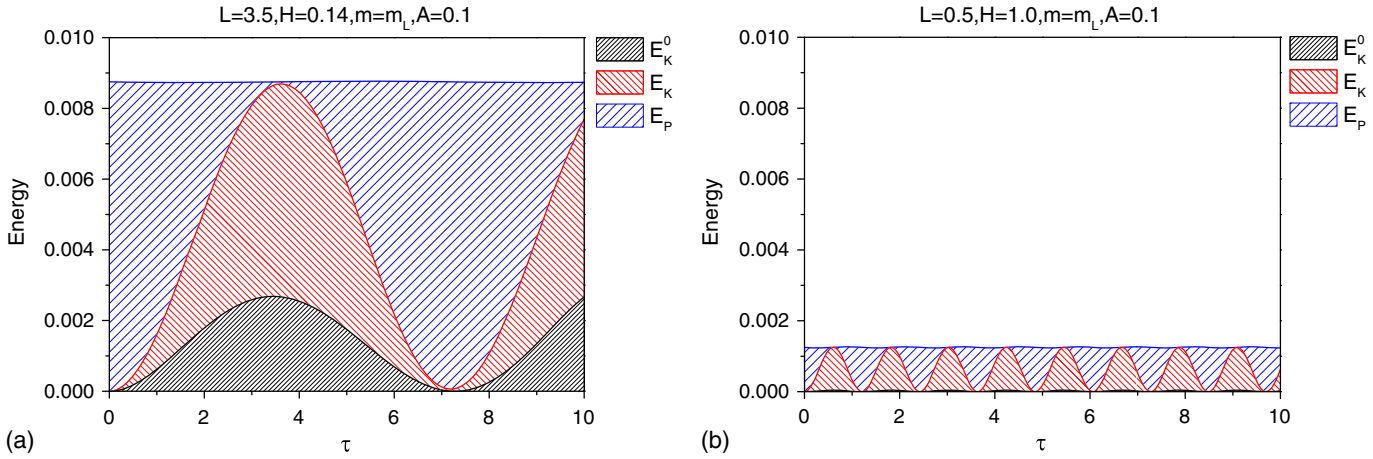

Fig. 12. Energy analysis for single-tank vessel, with initial free-surface deformation of Mode-1, for $m = m_L = 0.5$ and $A = 0.1$: (a) $H = 0.14$; (b) $H = 1.0$

$$A_c = \frac{\rho g}{(m + m_L)} B_j^1 \overline{\zeta}_j^1 = \frac{\rho g}{(m + m_L)} B_j^1 A, \quad \text{for } j = 1 \qquad (47)$$

Because B_1^1 is of order $O(L^2)$, referring to Eqs. (31) and (36), the vessel with a longer tank (i.e., shallower liquid depth) would have a larger displacement amplitude A_c. From an energy point of view, with the same initial free-surface amplitude, the initial potential energy in the shallower tank has a larger value, according to Eq. (30). This is confirmed in Fig. 12, in which the mechanical energy in the tank of depth $H = 0.14$ and $H = 1.0$ is compared. From Fig. 12, it is known that the initial potential energy of the fluid could totally transfer to the kinetic energy of the vessel and fluid. The maximum kinetic energy occurs when the potential energy becomes zero. It is interesting to discuss the partition of the vessel and fluid kinetic energy when the potential energy is totally transformed to the kinetic one. Fig. 13 shows the percentage of the

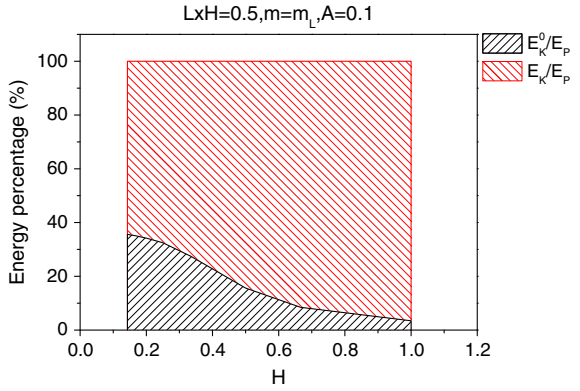

Fig. 13. Effect of tank configuration on percentage of maximum kinetic energy for single-tank vessel, with initial free-surface deformation of Mode-1, for $m = m_L = 0.5$ and $A = 0.1$

fluid and vessel kinetic energy. A major proportion of the initial potential energy is transformed to the fluid kinetic energy. Further, as the depth of the same amount of liquid decreases, the percentage of the vessel kinetic energy would increase. In other words, when the same amount of potential energy is input into the same amount of liquid on the same vessel, the vessel with shallower liquid tends to have greater oscillation amplitudes. This could be understood with the help of Eq. (47). The expression of the initial potential energy of Mode-1 could be derived easily. It can be seen that, with the same potential energy, the initial wave amplitude A is inversely proportional to the tank length L. Meanwhile, B_1^1 is of order $O(L^2)$, which leads to the fact that A_c is in proportion to L. Thus, even with the same amount of potential energy input, the vessel with a longer tank (i.e., shallower liquid depth) could also have a larger displacement amplitude.

Effects of Initial Free-Surface Deformation

In the previous three cases, the initial free-surface deformation is of the fundamental mode, which leads to a nearly harmonic vessel motion. In the fourth case, effects of the initial free-surface profile on the vessel motion are investigated. The vessel with a liquid tank of the dimension $L = B = 1$ and mean liquid depth $H = 0.5$ is considered. The initial free-surface profiles are of different modes with $j = 1, 3, 5$ and 7 in Eq. (46). Fig. 14 illustrates the initial liquid geometry in a tank with free-surface profiles of the first four modes. The amplitude of the profiles is fixed as $A = 0.1$. The vessel mass satisfies $m = m_L$.

Fig. 15(a) shows the free-surface elevation histories along the right tank wall. The amplitude of free-surface elevations in all cases are of the same order, regardless of the modes. Fig. 15(b) shows the history of the vessel displacement. It is found that the vessel with a higher-mode initial free-surface deformation has a smaller displacement amplitude. This is interesting, based on the fact that the free-surface deformations of all these modes could provide the same initial input of the potential energy, as shown in Fig. 16. Eq. (47) is used to explain this. The value of B_j^1 decreases as j grows, leading to the reduction of the displacement amplitude A_c. The motion process may be described, in detail. Consider the process of the vessel moving left. On the one hand, the averaged pressure amplitude along the tank wall in the case of Mode-1 is larger. On the other hand, the free-surface oscillation period of Mode-1 case is larger, which means that the acting time on the tank wall is larger. Thus, according to the theorem of momentum, the vessel of Mode-1 would have the largest motion. Also, from the evolution of all mechanical-energy components, it is obvious that the vessel of Mode-1 has the largest kinetic energy.

It is noticed that the vessel in the cases of Mode-2, Mode-3, and Mode-4 no longer oscillates harmonically and could move to the right hand side of its initial position, which is distinct from observations in the case of Mode-1. The spectra of these displacement histories are shown in Fig. 17. The natural frequencies of the

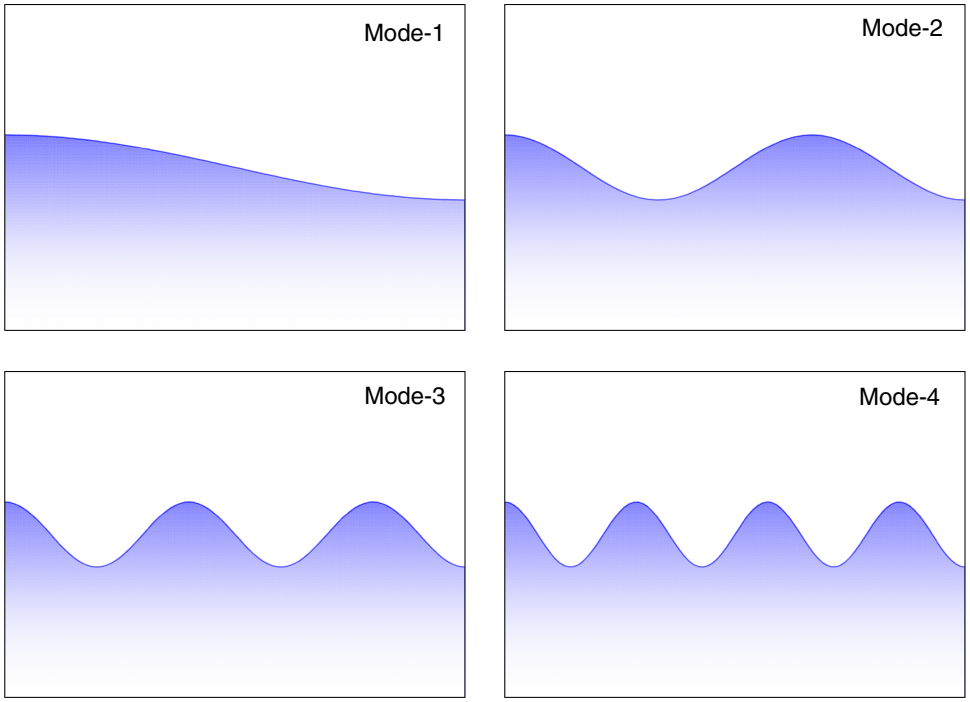

Fig. 14. Liquid geometry with free-surface deformation of Mode-1, Mode-2, Mode-3, and Mode-4

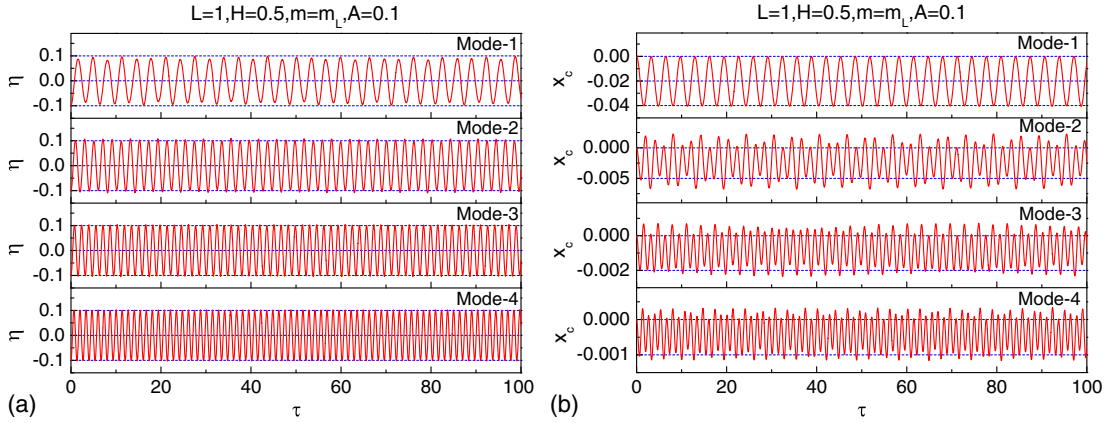

Fig. 15. Effect of initial free-surface deformation on single-tank vessel, for $L = 1$, $H = 0.5$, $m = m_L$, and $A = 0.1$: (a) wave elevation along the right tank wall; (b) vessel displacement

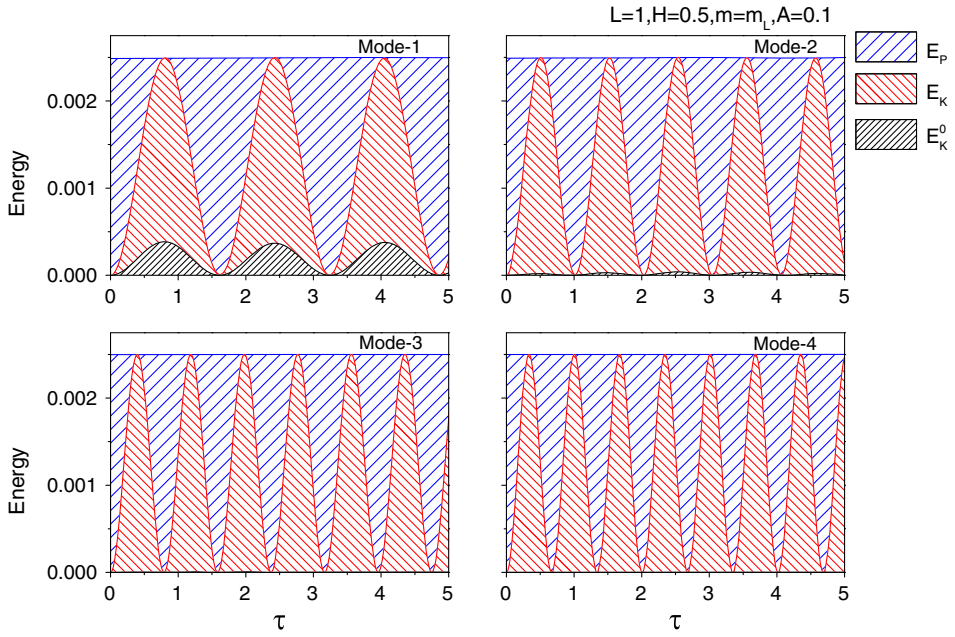

Fig. 16. Effect of initial free-surface deformation on energy components of single-tank vessel, for $L = 1$, $H = 0.5$, $m = m_L$, and $A = 0.1$

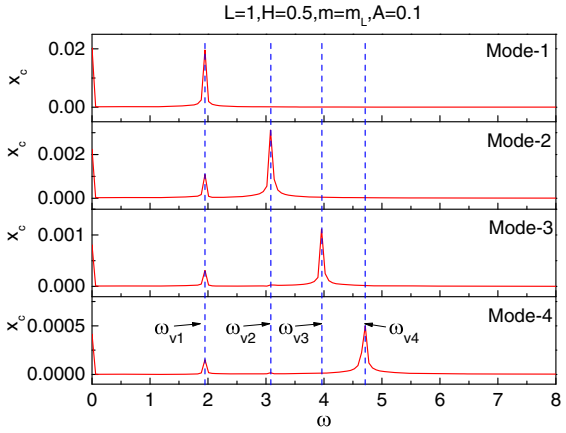

Fig. 17. Effect of initial free-surface deformation on spectrum of single-tank vessel oscillation, for $L = 1$, $H = 0.5$, $m = m_L$, and $A = 0.1$

coupling system shown in Fig. 6(b) are also marked in Fig. 17. It is found that the vessel oscillation frequencies are at the natural frequencies of the coupling system. At the natural frequency that is closest to the corresponding natural sloshing frequency ω_i of Mode-i, the natural mode has the largest amplitude. For cases of Mode-2 to Mode-4, the natural frequency ω_{v1} is also visible. This is also because of the initial conditions. As mentioned previously, the defined initial free-surface deformation is not the true free-surface mode of this coupling system. The coexistence of multiple frequency components also explains the wiggles in vessel displacement histories for cases of Mode-2–Mode-4 in Fig. 15. However, the corresponding wave elevation histories seem to be very stable. This is related to the fact that the vessel displacement is too small to affect the free surface evidently. As the vessel displacement grows to a sufficiently large amplitude (e.g., for the case of Mode-1), the vessel motion could have visible influences on the free surface and lead to nonharmonic wave elevation histories.

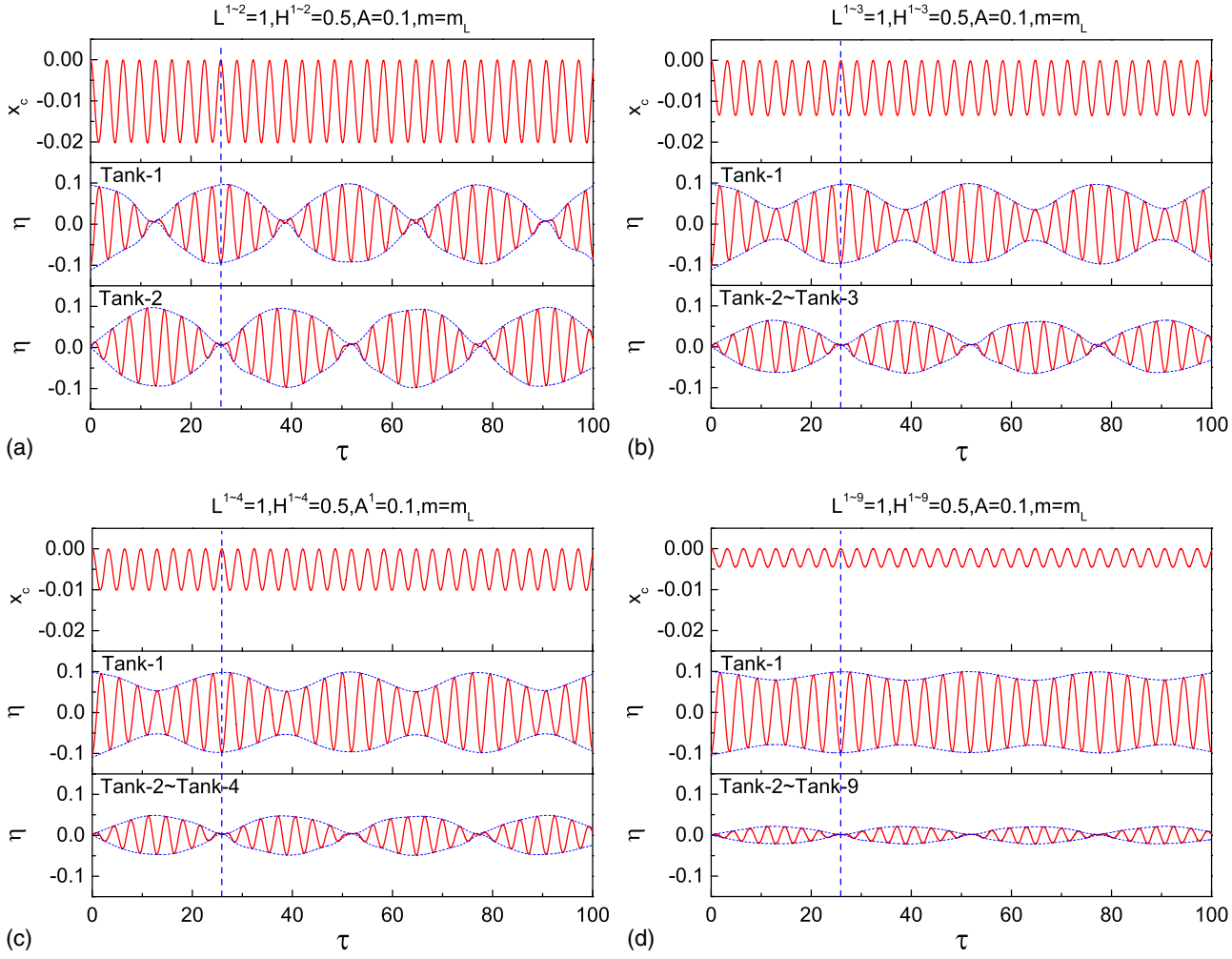

Fig. 18. Displacement of multiple-tank vessel and wave elevation along the right tank wall, with initial free-surface deformation of Mode-1 in Tank-1, for $L^k = 1$, $H^k = 0.5$, $m = m_L$, and $A = 0.1$: (a) 2-tank vessel; (b) 3-tank vessel; (c) 4-tank vessel; (d) 9-tank vessel

Free Motion of Vessel with Multiple Liquid Tanks

In this section, the coupling between vessel motion and liquid sloshing in multiple tanks is considered. For convenience, tanks with the initial free-surface disturbance are called the drive tanks, and the rest tanks are the response tanks. In fact, there exist practical situations when the vessel with drive tanks might be used as an approximation model. For example, when the LNG carrier experiences offshore loading or unloading operations, tanks with the liquid injected or drawn can be taken as drive tanks, whereas the other tanks are response tanks.

Effects of Number of Tanks

In the first case, effects of the number of liquid tanks are investigated. In this subsection, all tanks have the same dimension $L^k = B^k = 1$ and mean liquid depth $H^k = 0.5$. Initially, the liquid in Tank-1 has a free-surface deformation of Mode-1 with amplitude $A = 0.1$, whereas the rest tanks hold still liquid of a flat free surface. The mass of the vessel equals that of the overall liquid. Fig. 18 concerns the 2-, 3-, 4- and 9-tank vessel, in which the vessel displacement and wave elevation histories in all tanks are given. It is found that vessel motions are still nearly harmonic as the single-tank case. As the tank number increases, the amplitude of the vessel motion tends to reduce. This is expectable: (1) for vessels with more tanks, the same initial potential energy is transformed to the mechanical energy in more tanks besides the kinetic energy of the vessel itself; and (2) the vessel with more tanks is given a larger mass. For all vessels, the maximum wave amplitude in Tank-1 keeps the same, which is mainly depending on the initial free-surface amplitude. However, the elevation histories have evident envelopes, which is an obvious difference from the observation in the single-tank vessel. For the rest tanks, the maximum wave amplitude decreases as the tank number grows. For a more clear comparison, the envelopes of these free-surface elevation histories are abstracted and shown in Fig. 19. It is found that these envelopes have the same period. The envelope in response tanks is half-period delayed compared to that in Tank-1. As the number of tanks increases, the variation of the envelope curve in Tank-1 becomes gentler, and the envelope amplitude in the rest tanks decreases.

Fig. 20 shows several typical free-surface profiles in the 2-tank vessel within the first two periods for illustration purpose.

It is known that the envelope usually suggests that more than one wave components coexist in the fluid system. Thus, the FFT is performed on time history curves of Fig. 18. The obtained spectra are shown in Fig. 21. In all cases, the vessel oscillates at the same frequency ω_v. From the diagram of $\det[M(\omega)]$ in Fig. 22, it could also be confirmed that ω_v is a natural frequency of the coupling system. The natural frequency ω_v is independent of the number

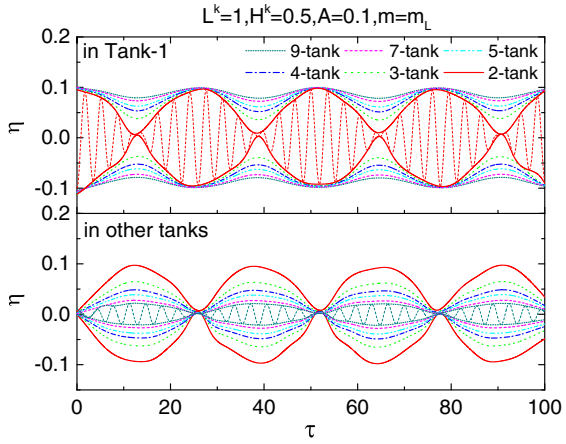

Fig. 19. Effect of tank number on wave elevation envelopes in multiple-tank vessel, with initial free-surface deformation of Mode-1 in Tank-1, for $L^k = 1$, $H^k = 0.5$, $m = m_L$, and $A = 0.1$

of tanks in this situation. However, the wave elevation in all tanks is dominated by both the lowest natural sloshing frequency ω_1 and the vessel motion frequency ω_v. In Tank-1, the amplitude of the wave component at ω_1 increases as the tank number grows. In the response tanks, two wave components have similar amplitudes. Adding waves of these two different frequencies would lead to the well-known beating behavior, which is featured by periodic envelopes, as shown in Figs. 18 and 19. The beat frequency is determined by the difference of two wave frequencies.

Fig. 23 further gives the mechanical energy variation of the liquid in tanks. For the 2-tank vessel, the mechanical energy in Tank-1 could totally transfer to the liquid in Tank-2. This explains the observation in Fig. 18(a), in which the maximum wave amplitudes in two tanks are the same. However, for a vessel with more than two tanks, the mechanical energy in Tank-1 could not reach zero. In other words, the mechanical energy in Tank-1 could not totally transfer to the liquid in other tanks. Fig. 24 gives the maximum mechanical energy of liquid in the rest tanks. The percentage is obtained by comparing with the initial potential energy in Tank-1. The mechanical energy percentage in Tank-2 is also marked in the figure. It is found that, for the vessel with more tanks, the mechanical energy is less likely to transfer out of Tank-1. Thus, even for a vessel with identical liquid tanks, the initial input of the mechanical energy does not have to distribute equally in all tanks.

Effects of Vessel Mass

Fig. 23 has shown that the mechanical energy in Tank-1 could transfer totally to the liquid in Tank-2 for the 2-tank vessel. It is necessary to investigate whether this property remains for the vessel with a different mass. Fig. 25 shows four different cases when the

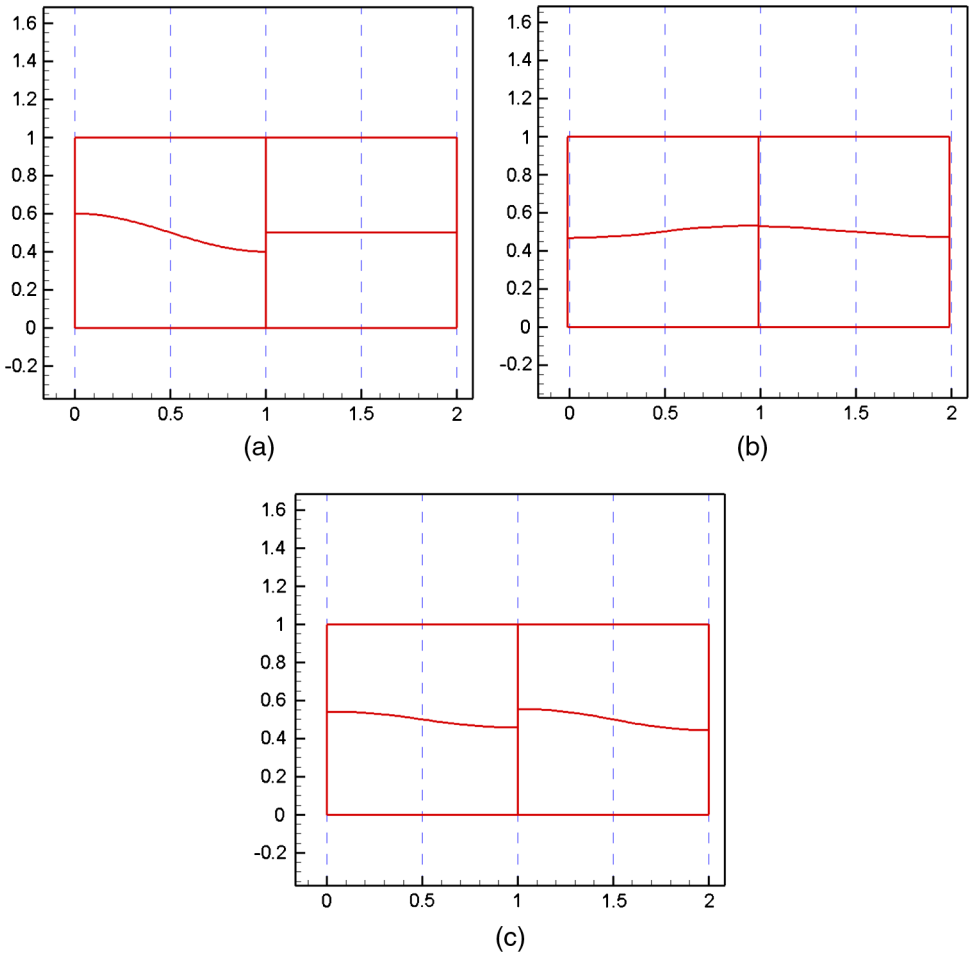

Fig. 20. Position and free-surface profiles of 2-tank vessel, with initial free-surface deformation of Mode-1 in Tank-1, for $L = 1$, $H = 0.5$, $m = m_L$, and $A = 0.1$, at: (a) $\tau = 0$; (b) $\tau = 2.40$; (c) $\tau = 6.40$

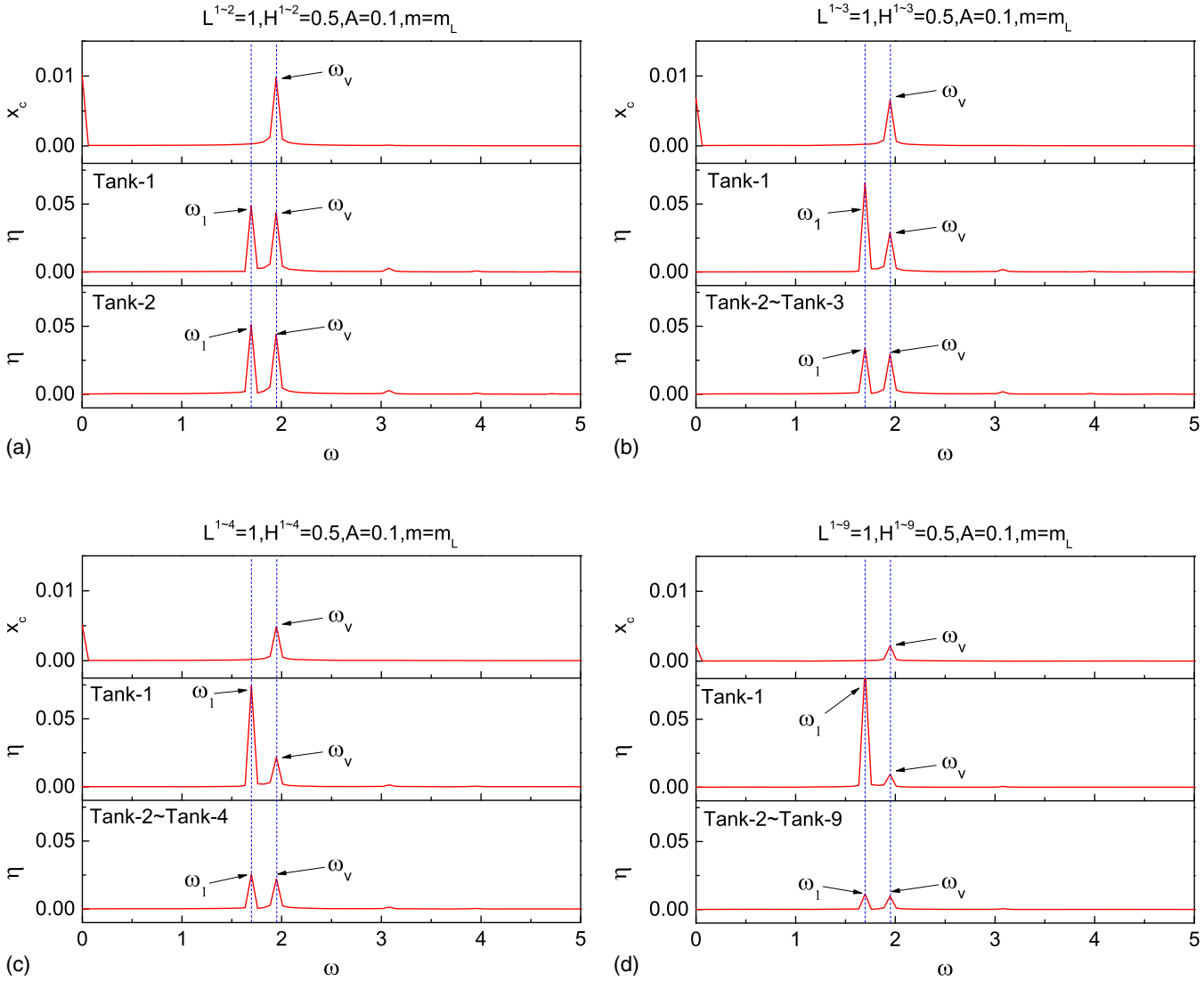

Fig. 21. Spectrum of displacement of multiple-tank vessel and wave elevation in tanks, with initial free-surface deformation of Mode-1 in Tank-1, for $L^k = 1$, $H^k = 0.5$, $m = m_L$, and $A = 0.1$: (a) 2-tank vessel; (b) 3-tank vessel; (c) 4-tank vessel; (d) 9-tank vessel

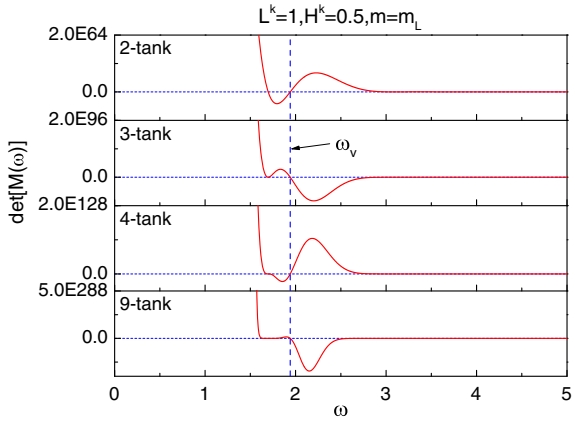

Fig. 22. Diagram of det$[M(\omega)]$ of multiple-tank vessel, for $L^k = 1$, $H^k = 0.5$, and $m = m_L$

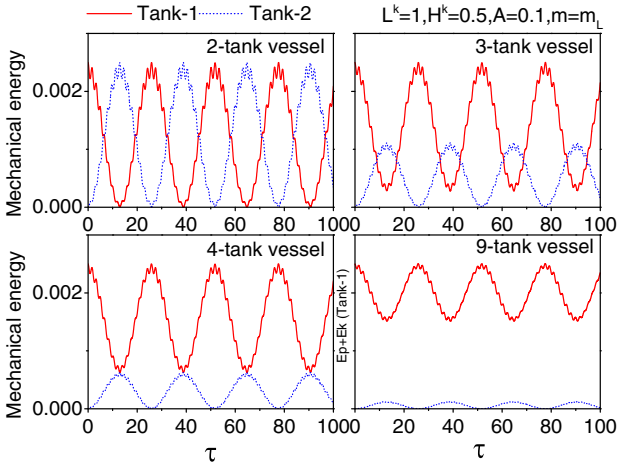

Fig. 23. Mechanical energy of liquid in Tank-1 and Tank-2 of multiple-tank vessel, with initial free-surface deformation of Mode-1 in Tank-1, for $L^k = 1$, $H^k = 0.5$, $m = m_L$, and $A = 0.1$

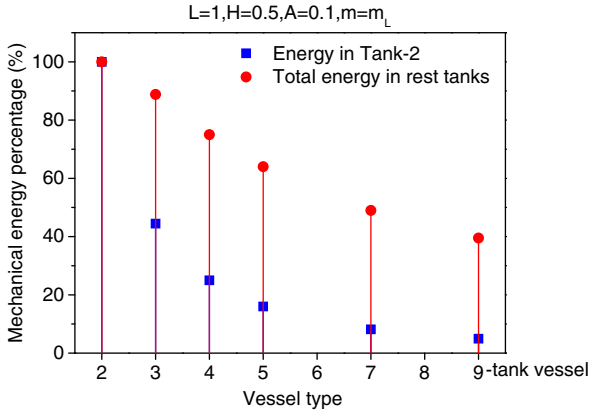

Fig. 24. Maximum mechanical energy of liquid in response tanks of multiple-tank vessel, with initial free-surface deformation of Mode-1 in Tank-1, for $L^k = 1$, $H^k = 0.5$, $m = m_L$, and $A = 0.1$

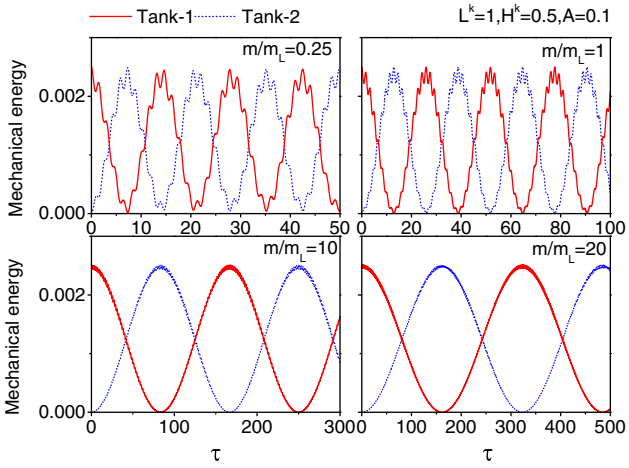

Fig. 26. Effect of vessel mass on mechanical energy of liquid in 2-tank vessel, with initial free-surface deformation of Mode-1 in Tank-1, for $L^k = 1$, $H^k = 0.5$, and $A = 0.1$

vessel mass changes from $m = 0.25m_L$ to $m = 20m_L$. In all cases, the vessel oscillates nearly harmonically. Wave elevations in both tanks have shown evident envelopes. These envelopes have the same maximum amplitude but different periods. Generally, the envelope period for a heavier vessel is larger. The fluid energy in two tanks is compared in Fig. 26. This confirms that, for a vessel with two tanks that have the same dimension and mean liquid depth, there could be an instant when the mechanical energy in one tank totally transfers to the other.

Vessels with more than two tanks are of further concern. Frequencies and amplitudes of vessel motions are shown in Fig. 27. For vessels with tanks that have the same dimension and mean liquid depth, if the mass ratio between the vessel and overall liquid is fixed, the vessel motion frequency would always be the same. The motion amplitude of a vessel with N tanks is N times smaller than that of the single-tank vessel.

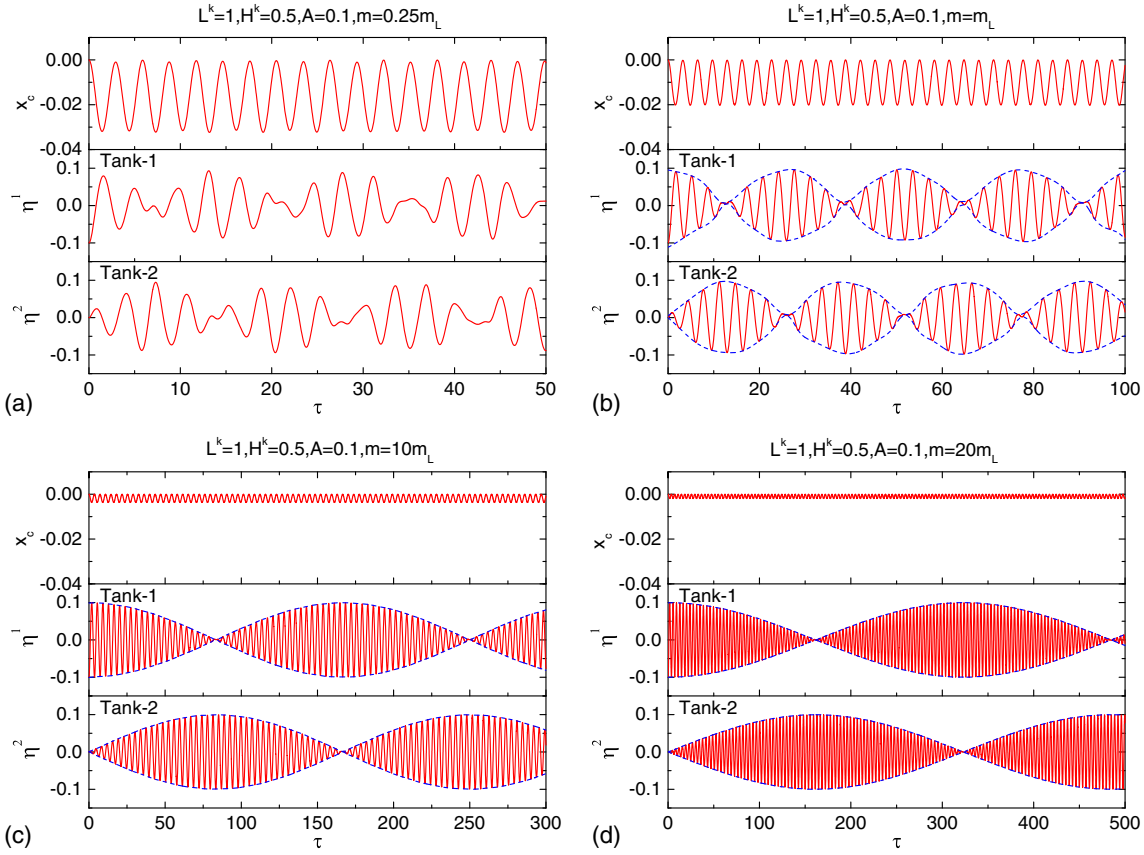

Fig. 25. Effect of vessel mass on displacement of 2-tank vessel and wave elevation in tanks, with initial free-surface deformation of Mode-1, for $L^k = 1$, $H^k = 0.5$, and $A = 0.1$: (a) $m = 0.25m_L$; (b) $m = m_L$; (c) $m = 10m_L$; (d) $m = 20m_L$

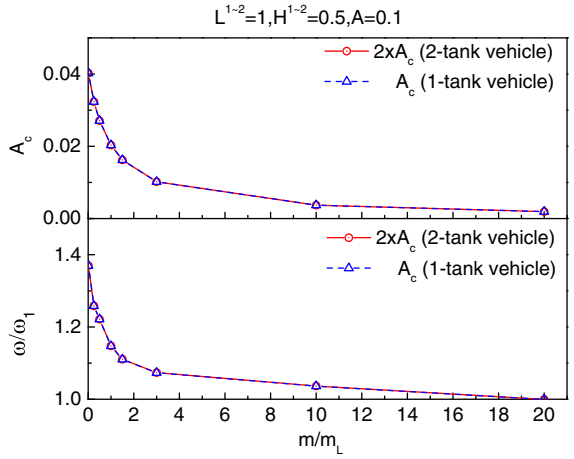

Fig. 27. Effect of vessel mass on oscillation amplitude and frequency of multiple-tank vessel, with initial free-surface deformation of Mode-1 in Tank-1, for $L^k = 1$, $H^k = 0.5$, and $A = 0.1$

Effects of Number of Drive Tanks

The third case concerns the vessel with a different number of drive tanks. Fig. 28 shows the vessel displacement and wave elevations in all tanks for the 4-tank vessel with 1, 2, or 3 drive tanks. It is found that the vessel displacement amplitude increases as the number of drive tanks increases. This is easily expected because the vessel with more drive tanks has larger potential energy as initial input. These vessel oscillations have the same frequencies, which are not affected by the number of drive tanks. In different tanks, wave elevations have the envelopes. The maximum wave elevation in drive tanks are the same. However, in the response tanks, the maximum wave amplitude grows as the number of drive tanks increases. Here, N_{dri} and N_{res} are used to denote the number of drive tanks and that of response tanks, respectively. It is found that, in the case of $N_{\text{dri}} < N_{\text{res}}$, the maximum wave amplitude in response tanks is smaller than that in drive tanks. On the other hand, in the case of $N_{\text{dri}} > N_{\text{res}}$, the maximum wave amplitude in response tanks is greater than that in drive tanks. A special situation is when $N_{\text{dri}} = N_{\text{res}}$. In this situation, the maximum wave amplitude in all tanks is the same. Fig. 28(b) is very similar to Fig. 18(a) in terms of the 2-tank vessel. Thus, it is known that the mass proportion of the liquid in drive and response tanks could affect the free-surface behaviors.

The mechanical energy of the fluid in each tank is shown in Fig. 29. It is found that when the vessel has fewer drive tanks, the maximum fluid mechanical energy in any response tank is smaller than that in each drive tank. As the number of drive tanks becomes larger, the fluid energy in each response tank increases. For a vessel with more drive tanks, the fluid energy in a response tank could exceed the maximum mechanical energy in a drive tank. This is linked to the fact that the mechanical energy in response tanks is dependent on the vessel motion amplitude. For a vessel with more drive tanks, the vessel could have a larger displacement, which means that the excitation on the liquid in response tanks is stronger. Thus, more violent fluid motion would occur in response tanks. For the special case of $N_{\text{dri}} = N_{\text{res}}$, the

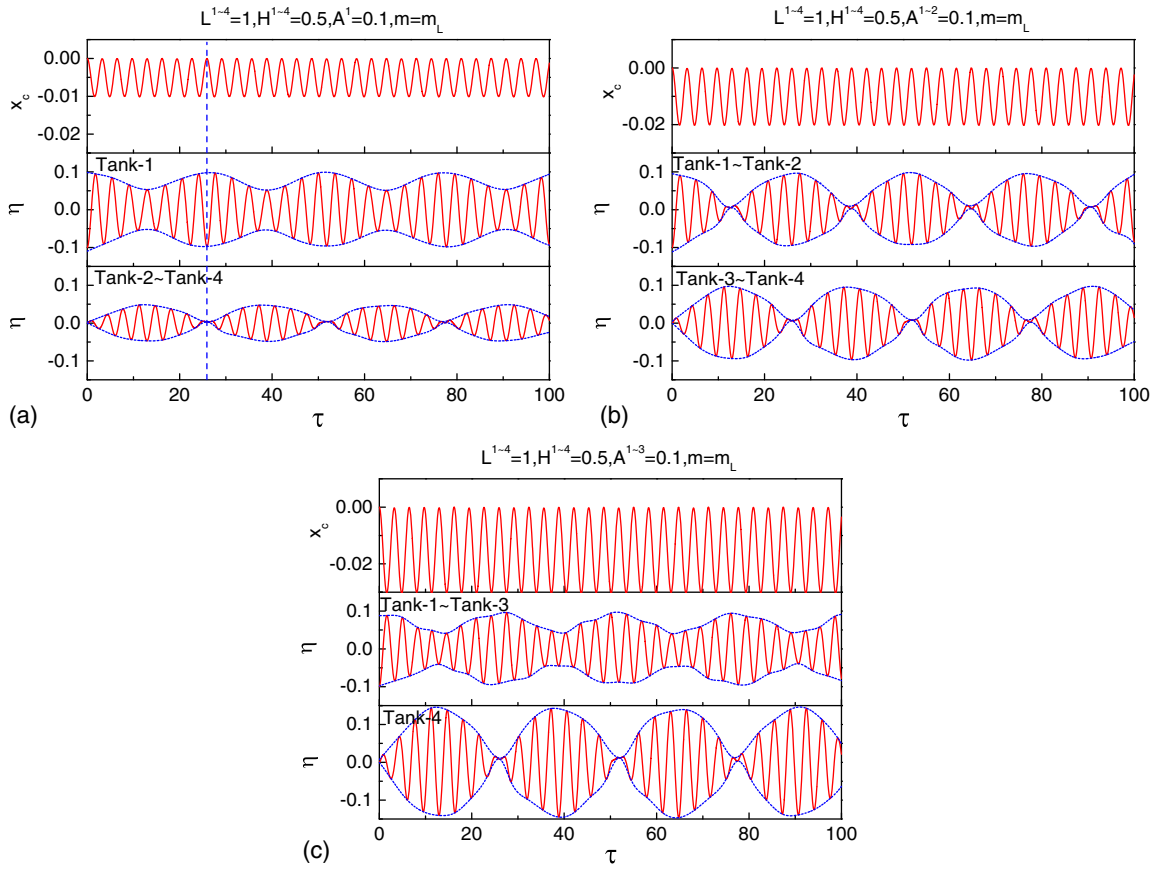

Fig. 28. Effect of number of drive tanks on displacement of 4-tank vessel and wave elevation in tanks, with initial free-surface deformation of Mode-1, for $L^k = 1$, $H^k = 0.5$, and $m = m_L$: (a) $A^1 = 0.1$; (b) $A^{1\sim2} = 0.1$; (c) $A^{1\sim3} = 0.1$

J. Eng. Mech., 2016, 142(7): -1--1

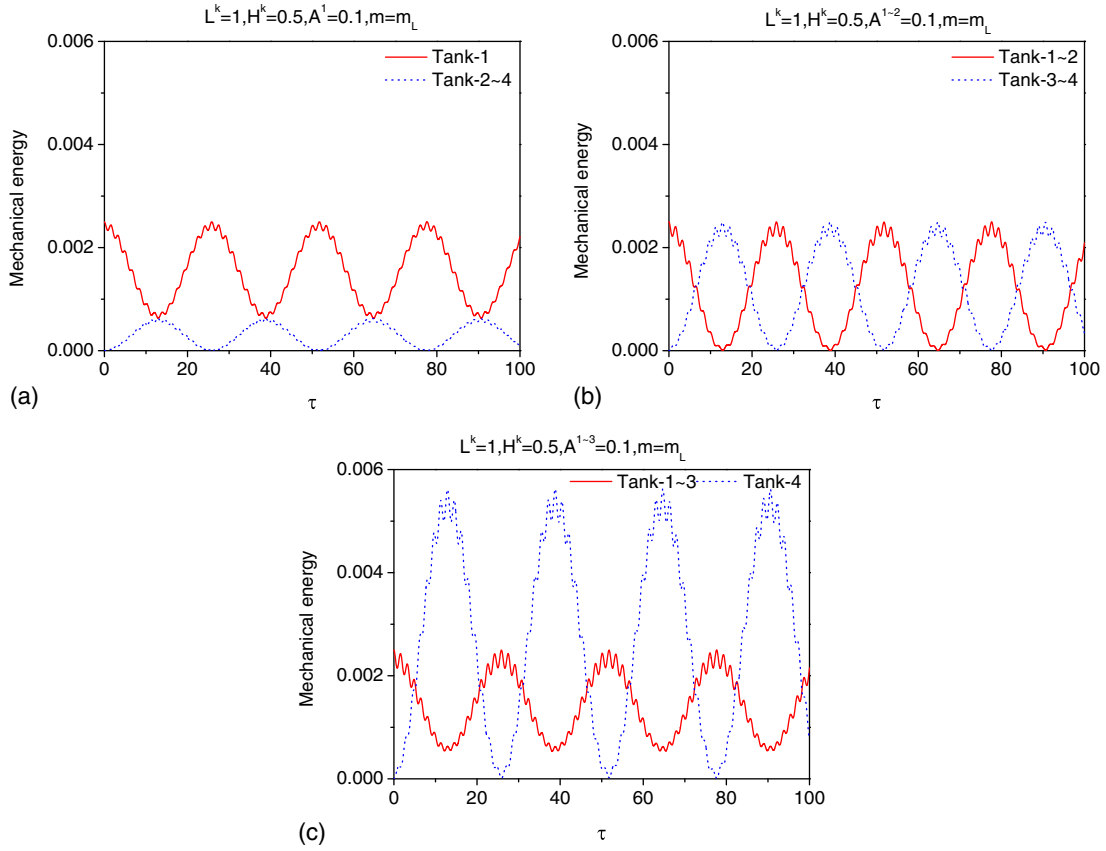

Fig. 29. Effect of number of drive tanks on mechanical energy of liquid in 4-tank vessel, with initial free-surface deformation of Mode-1, for $L^k = 1$, $H^k = 0.5$, and $m = m_L$: (a) $A^1 = 0.1$; (b) $A^{1\sim2} = 0.1$; (c) $A^{1\sim3} = 0.1$

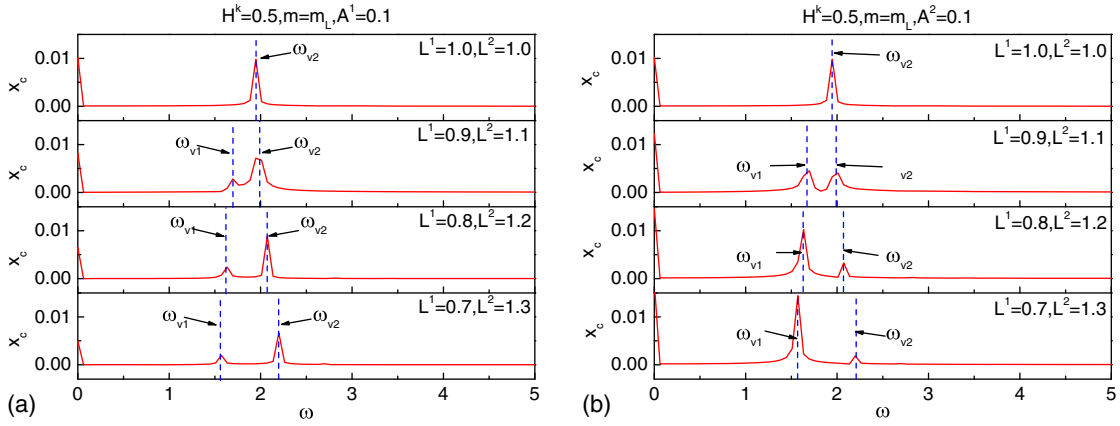

Fig. 30. Effect of tank configuration on spectrum of displacement of 2-tank vessel, with initial free-surface deformation of Mode-1, for $H^k = 0.5$ and $m = m_L$: (a) $A^1 = 0.1$; (b) $A^2 = 0.1$

mechanical energy in drive and response tanks would have the same amplitude.

Vessel with Tanks of Different Configuration

In the fourth case, the vessel has tanks of different configuration. The vessel mass is equal to the total mass of the liquid. Firstly, the total liquid is divided into 2 tanks with the same liquid depth $H = 0.5$. So, the tank configuration is only determined by the tank length. Vary the length of Tank-1 from 0.7 to 1.0 and correspondingly the length of Tank-2 from 1.3 to 1.0. Figs. 30(a and b) consider the case when the drive tanks are set as Tank-1 and Tank-2, respectively. The spectra of the vessel displacements are given. Two frequency components primarily contribute to the vessel oscillations. From the diagram of $\det[M(\omega)]$ in Fig. 31, it is confirmed that both of them are natural frequencies of the coupling system. This is not a surprise because the linear solution could always be expressed as a summation of the natural modes. However, the amplitude of each

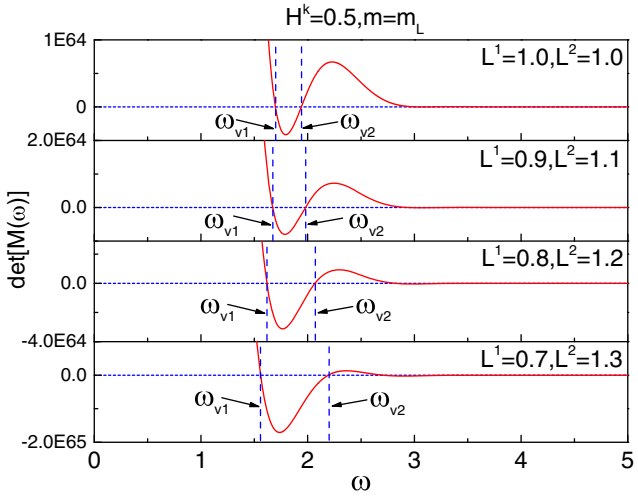

Fig. 31. Effect of tank configuration on diagram of det$[M(\omega)]$ of 2-tank vessel, for $H^k = 0.5$ and $m = m_L$

mode may vary for different initial conditions. The maximum natural mode occurs at the natural frequency closest to ω_1. Here, ω_1 denotes the dominant sloshing frequency in the stationary vessel, caused by the same initial free-surface deformation. For Fig. 30(a), the ω_1 associated with the initial free-surface deformation in Tank-1 is closest to the natural frequency ω_{v2} of the system so that the natural mode at ω_{v2} has the maximum amplitude. For Fig. 30(b), ω_1 is closet to ω_{v1}, and the maximum natural mode occurs at ω_{v1}. It is also found that these two dominant frequencies become more separated as the size difference of two tanks increases.

Then, Fig. 32 compares the time variation of the fluid mechanical energy in each tank. Figs. 32(a) and (b) illustrate the situation when the drive tanks are Tank-1 and Tank-2, respectively. For both situations, the fluid mechanical energy in one tank is less likely to transfer to the other, as the two tanks become more distinctive. Only when these two tanks are the same could the fluid mechanical energy in one tank transfer totally to the other.

Further consider the vessel with three different liquid tanks. The length of each tank is set as $L^1 = 0.8$, $L^2 = 1.0$, and $L^3 = 1.2$. Fig. 33(a) shows the histories of the vessel displacement when the drive tank is chosen to be Tank-1, Tank-2, and Tank-3, respectively. It is clear that the vessel displacement histories are no longer nearly harmonic. A different drive tank may lead to totally different vessel motions. The spectra of these vessel motion histories are shown in Fig. 33(b). The vessel motions could be expressed by three natural modes of the system, according to the diagram of det$[M(\omega)]$ in Fig. 33(c). As the drive tank varies from Tank-1 to Tank-3, the natural frequency closest to ω_1 becomes ω_{v3}, ω_{v2}, and ω_{v1}, respectively. Correspondingly, the natural mode at ω_{v3}, ω_{v2}, and ω_{v1} has the maximum amplitude, respectively.

Conclusions

In the present study, the pure coupling between the vessel motion and liquid sloshing in multiple tanks is considered. The vessel could move freely on the horizontal ground, and its motion is solely driven by the liquid sloshing in tanks. External disturbance factors (e.g., spring constraint or force field) that might affect oscillation characteristics of the system are not involved. The analytical solution for this coupling problem has been derived based on the potential flow theory. The way to determine natural frequencies of the coupling system is also given. Then, dynamic properties of the vessel with one or more rectangular tanks are studied systematically.

For the vessel with a single sloshing tank, effects of the initial free-surface deformation and vessel mass on the vessel displacement, free-surface elevation, and mechanical-energy components of the system have been discussed. For a system with constant liquid-vessel mass ratio, the tank dimensions could also affect the oscillation properties. With the same amount of potential energy as initial input to the fluid, the vessel with shallower liquid tends to have greater oscillation amplitude.

For a vessel with multiple tanks, supplementing tanks of the same geometry to the vessel does not change the vessel motion frequency. For convenience, tanks with initial free-surface disturbance are called the drive tanks, and the rest tanks are the response tanks. Only when the drive and response tanks have the same number, the mechanical energy in the drive tanks could totally transfer to the

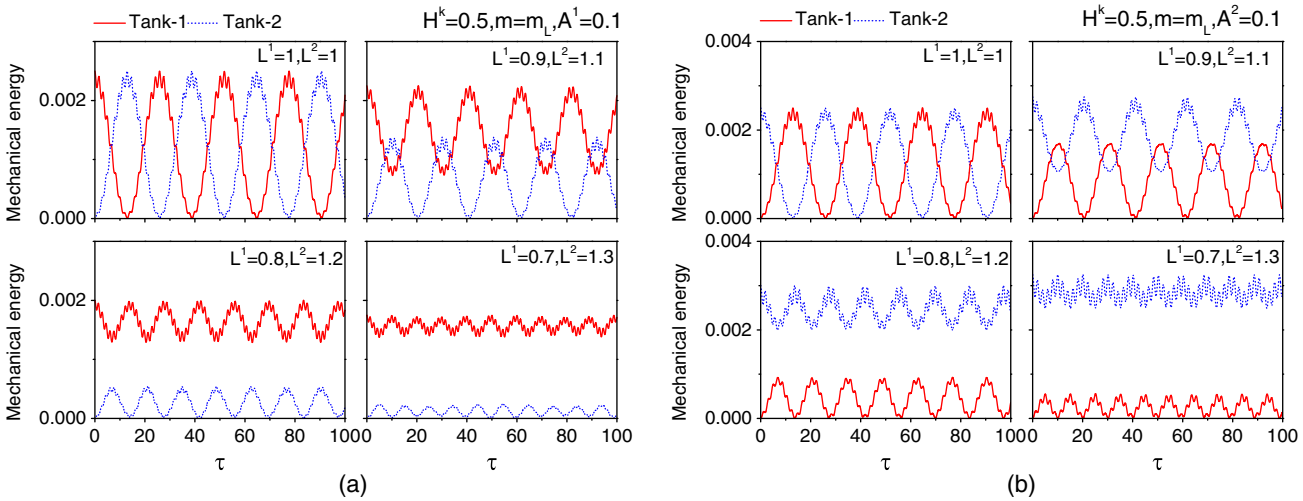

Fig. 32. Effect of tank configuration on mechanical energy of liquid in 2-tank vessel, with initial free-surface deformation of Mode-1, for $H^k = 0.5$ and $m = m_L$: (a) $A^1 = 0.1$; (b) $A^2 = 0.1$

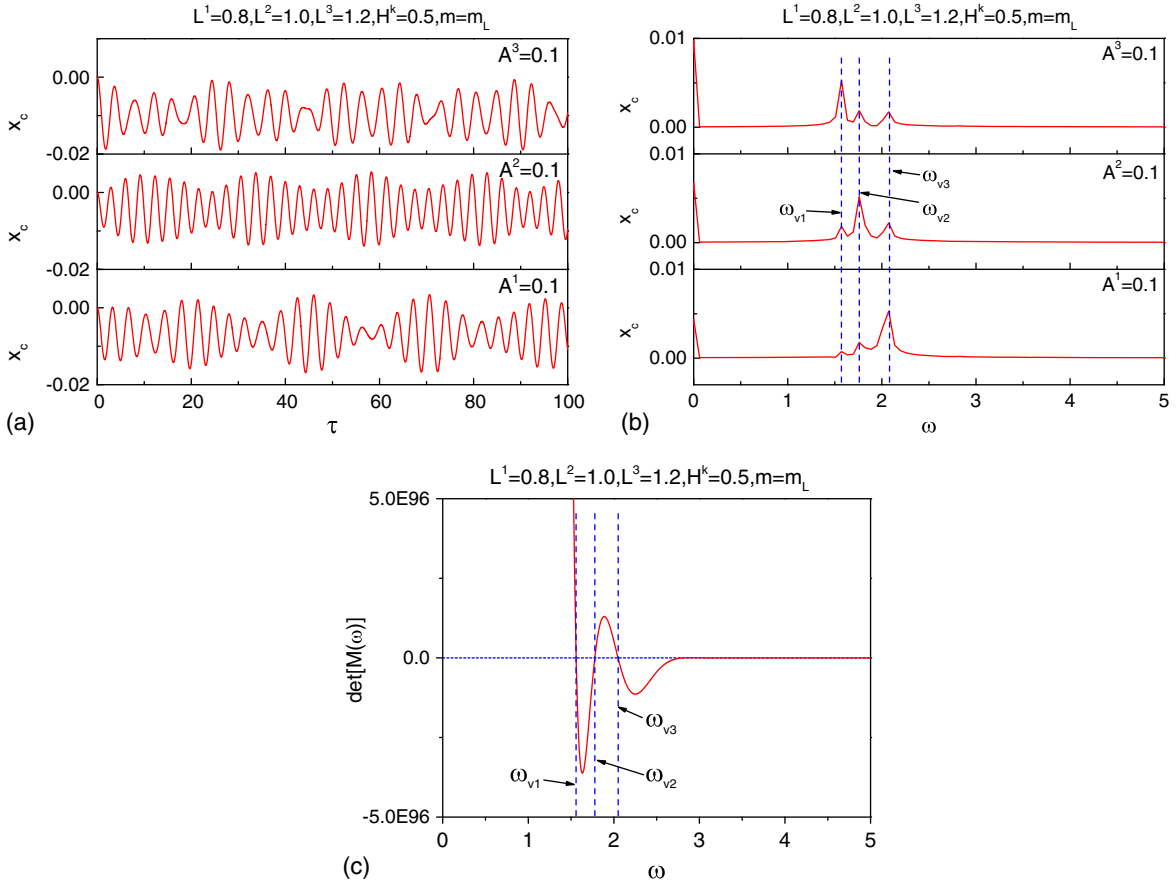

Fig. 33. Effect of tank configuration on displacement of 3-tank vessel, with initial free-surface deformation of Mode-1, for $L^1 = 0.8$, $L^2 = 1.0$, $L^3 = 1.2$, $H^k = 0.5$, and $m = m_L$: (a) vessel displacement; (b) spectrum of vessel displacement; (c) diagram of det$[M(\omega)]$

response ones. Otherwise, the mechanical energy in the drive tanks could not reach zero. For the vessel with different tanks, the fluid mechanical energy in the drive tanks is less likely to transfer to the response tanks because dimensions of tanks become more distinctive.

Acknowledgments

The author gratefully acknowledges the financial support from the Lloyd's Register Foundation (LRF) through the joint center involving University College London, Shanghai Jiao Tong University, and Harbin Engineering University. The LRF helps to protect life and property by supporting engineering-related education, public engagement, and the application of research. This work is also supported by the China Scholarship Council (CSC) (No. 201206680001). Thanks also go to Prof Guo Xiong Wu from University College London for valuable discussions.

References

Alemi Ardakani, H., and Bridges, T. J. (2010). "Dynamic coupling between shallow-water sloshing and horizontal vehicle motion." *Eur. J. Appl. Math.*, 21(6), 479–517.

Alemi Ardakani, H., Bridges, T. J., and Turner, M. R. (2012). "Resonance in a model for Cooker's sloshing experiment." *Eur. J. Mech. B-Fluid.*, 36, 25–38.

Cooker, M. J. (1994). "Water waves in a suspended container." *Wave Motion*, 20(4), 385–395.

Frandsen, J. B. (2005). "Numerical predictions of tuned liquid tank structural systems." *J. Fluid. Struct.*, 20(3), 309–329.

Gavrilyuk, I., et al. (2012). "Multimodal method for linear liquid sloshing in a rigid tapered conical tank." *Eng. Comput.*, 29(2), 198–220.

Herczynski, A., and Weidman, P. D. (2012). "Experiments on the periodic oscillation of free containers driven by liquid sloshing." *J. Fluid Mech.*, 693, 216–242.

Ikeda, T., and Nakagawa, N. (1997). "Non-linear vibrations of a structure caused by water sloshing in a rectangular tank." *J. Sound Vibr.*, 201(1), 23–41.

Kim, Y., et al. (2007). "Study on coupling effects of ship motion and sloshing." *Ocean Eng.*, 34(16), 2176–2187.

Malenica, S., Zalar, M., and Chen, X. B. (2003). "Dynamic coupling of seakeeping and sloshing." *Proc., 13th ISOPE*, ISOPE, Hawaii.

Mitra, S., et al. (2012). "A 3D fully coupled analysis of nonlinear sloshing and ship motion." *Ocean Eng.*, 39, 1–13.

Molin, B., et al. (2002). "LNG-FPSO's: Frequency domain, coupled analysis of support and liquid cargo motion." *Proc., 10th Congress of IMAM*, IMAM, Crete, Greece.

Newman, J. N. (2005). "Wave effects on vessels with internal tanks." *Proc., 20th IWWWFB*, Univ. of Oslo, Longyearbyen, Norway.

Rognebakke, O. F., and Faltinsen, O. M. (2003). "Coupling of sloshing and ship motions." *J. Ship Res.*, 47(3), 208–221.

Turner, M. R., Alemi Ardakani, H., and Bridges, T. J. (2015). "Instability of sloshing motion in a vessel undergoing pivoted oscillations." *J. Fluid. Struct.*, 52, 166–180.

Turner, M. R., and Bridges, T. J. (2013). "Nonlinear energy transfer between fluid sloshing and vessel motion." *J. Fluid Mech.*, 719, 606–636.

Turner, M. R., Bridges, T. J., and Alemi Ardakani, H. (2013). "Dynamic coupling in Cooker's sloshing experiment with baffles." *Phys. Fluids*, 25(11), 112102.

Weidman, P. D. (2005). "Sloshing in suspended containers." *Proc., APS 58th Annual Meeting of the Division of Fluid Dynamics*, APS, Chicago.

Yu, J. (2015). "Effects of finite water depth on natural frequencies of suspended water tanks." *Stud. Appl. Math.*, 125, 337–391.
Zhang, C. (2015a). "Analysis of liquid sloshing in LNG carrier with wedge-shaped tanks." *Ocean Eng.*, 105, 304–317.
Zhang, C. (2015b). "Application of an improved semi-Lagrangian procedure to fully-nonlinear simulation of sloshing in non-wall-sided tanks." *Appl. Ocean Res.*, 51, 74–92.
Zhang, C., Li, Y., and Meng, Q. (2015). "Fully nonlinear analysis of second-order sloshing resonance in a three-dimensional tank." *Comput. Fluids.*, 116, 88–104.
Zhao, W., Yang, J., Hu, Z., and Tao, L. (2014). "Coupled analysis of nonlinear sloshing and ship motions." *Appl. Ocean Res.*, 47, 85–97.
Zhao, W., Yang, J., Hu, Z., and Wei, Y. (2011). "Recent developments on the hydrodynamics of floating liquid natural gas (FLNG)." *Ocean Eng.*, 38(14–15), 1555–1567.